Greedy Bayesian Posterior Approximation with Deep Ensembles

Anonymous authors
Paper under double-blind review

Abstract

Ensembles of independently trained neural networks are a state-of-the-art approach to estimate predictive uncertainty in Deep Learning, and can be interpreted as an approximation of the posterior distribution via a mixture of delta functions. The training of ensembles relies on non-convexity of the loss landscape and random initialization of their individual members, making the resulting posterior approximation uncontrolled. This paper proposes a novel and principled method to tackle this limitation, minimizing an f-divergence between the true posterior and a kernel density estimator (KDE) in a function space. We analyze this objective from a combinatorial point of view, and show that it is submodular with respect to mixture components for any f. Subsequently, we consider the problem of greedy ensemble construction. From the marginal gain on the negative f-divergence, which quantifies an improvement in posterior approximation yielded by adding a new component into the KDE, we derive a novel diversity term for ensemble methods. The performance of our approach is demonstrated on computer vision out-of-distribution detection benchmarks in a range of architectures trained on multiple datasets. The source code of our method is made publicly available.

1 Introduction

Estimation of predictive uncertainty is one of the most important challenges to solve in Deep Learning (DL). Applications in finance, medicine and self-driving cars are examples where reliable uncertainty estimation may help to avoid substantial financial losses, improve patient outcomes, or prevent fatal accidents (Gal, 2016). However, to date, despite rapid progress, there is a lack of principled methods that reliably estimate the predictive uncertainty of deep neural networks (DNNs).

Bayesian approaches to Machine Learning generally offer great benefits, which provide out-of-the-box features such as model selection (Immer et al., 2021), uncertainty quantification Wilson & Izmailov (2020), and incorporation of prior knowledge into the models (Fortuin, 2021). From a Bayesian standpoint, for a model z trained on some data $\mathcal{D}$, there exist four main components: posterior $p(z \mid \mathcal{D})$, prior $p(z)$, likelihood $p(\mathcal{D} \mid z)$ and evidence $p(\mathcal{D})$. In this work we focus on the applications to uncertainty estimation, and thus are interested in a posterior distribution $p(z \mid \mathcal{D})$, assuming that it is multimodal (Wilson & Izmailov, 2020). This assumption is natural in the case of overparameterized models, such as DNNs.

Numerous attempts have been made to develop Bayesian techniques for posterior approximation and uncertainty estimation in DL (Gal & Ghahramani, 2016; Lakshminarayanan et al., 2017; Ciosek et al., 2019; Maddox et al., 2019; Izmailov et al., 2020; Van Amersfoort et al., 2020; Wenzel et al., 2020b; He et al., 2020; Wilson & Izmailov, 2020). One of the most practical and empirically best-performing approaches is based on training a series of independent DNNs (Lakshminarayanan et al., 2017; Wilson & Izmailov, 2020; Ashukha et al., 2020; Lu et al., 2020; Wenzel et al., 2020b). The main method in this category, *Deep Ensembles* (DE) (Lakshminarayanan et al., 2017), is used as a reference approach in the context of this paper.

Recent studies, e.g. Wilson & Izmailov (2020) interpret ensembles as an approximation of predictive posterior. While this interpretation is correct from a Bayesian point of view, obtaining individual ensemble members via maximum a posteriori probability (MAP) estimation, as e.g. done in DE (Lakshminarayanan et al., 2017), may not lead to obtaining good coverage of the full support of the posterior distribution, and has arbitrarily bad approximation guarantees. For

example, the resulting approximation can be poor in the case when the true posterior distribution is unimodal, skewed and long-tailed. In this work, we argue that enforcing coverage of posterior (i.e. ensemble diversity) is non-trivial, and needs a specialized principled approach. We highlight this graphically in Figure 1.

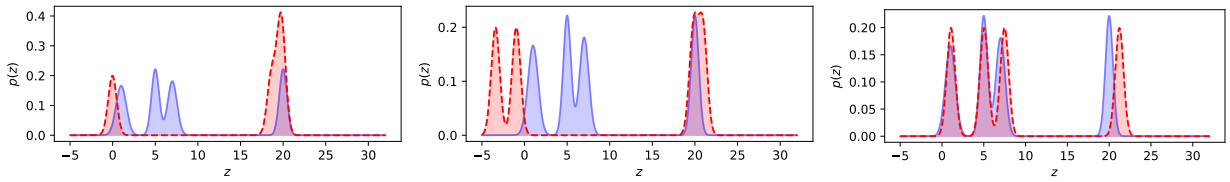

(a) (b) (c)

Figure 1: Illustration of how our method (c) approximates a 1D multimodal distribution $p(z)$ compared to a randomization-based mode picking (a), and naïve diversity training (b). Blue shows the true distribution and red – approximations. This figure can be reproduced using the provided source code.

Another important line of work in modern Bayesian DL (BDL) is a paradigm of performing Bayesian inference in the weight space. While distributions over weights induce distributions over functions (Wilson & Izmailov, 2020), it is rather unclear what the properties of such functions are, and whether Bayesian posteriors obtained in the weight space yield good quality approximations in the function space. For example, it is known that diverse weights do not necessary yield diverse functions, thus sampling from weight-based posteriors may yield poor quality uncertainty estimation, e.g. in detecting out-of-distribution (OOD) data (Garipov et al., 2018; Hafner et al., 2020).

Recent studies (Wang et al., 2019; D'Angelo & Fortuin, 2021) show the promise of particle optimization variational inference (POVI) done in the function space, however, the performance of those methods is not state-of-the-art due to the use of BNN weight priors. Specifically, in the BNN literature, enforcing prior only over weights and avoiding training techniques like batch-normalization Ioffe & Szegedy (2015) or mixup Zhang et al. (2018) is a de-facto standard, as these techniques have no Bayesian interpretation. In practice, a weight decay prior combined with batch normalization Ioffe & Szegedy (2015), data augmentation and dropout Gal & Ghahramani (2016) are often employed due to empirical improvement, and theoretical guarantees are traded for practical performance. Furthermore, particle-based function space VI requires training an ensemble of BNNs simultaneously, which is not only difficult to implement, but also requires extensive resources for parallelization.

Summary of the contributions. In this paper, we propose *a novel and principled* methodology for approximate function space posterior inference for DNNs. Contrary to the mainstream approach in BDL, which is based on defining a posterior distribution over the model parameters (Maddox et al., 2019), we take a functional view, which allows us to treat the problem of training ensembles as optimization over sets. Namely, selecting a set of functions to approximate the Bayesian posterior is fundamentally similar to problems such as facility location and set cover, which are frequently solved using submodular optimization (Krause et al., 2008). Specifically, our contributions are:

1. We show that fitting a kernel density estimator to a distribution using an f-divergence is a cardinality-fixed non-monotone submodular maximization problem.

2. Inspired by the Random Greedy algorithm for submodular maximization (Buchbinder et al., 2014), we design a new method for the function space Bayesian posterior approximation via greedy training of ensembles with a justified coverage-promoting diversity term.

3. We demonstrate the effectiveness and competitiveness of our approach compared to DE in the OOD detection task on MNIST, CIFAR, and SVHN, benchmarks on different architectures and ensemble sizes. Furthermore, we show that our method can use state-of-the-art training techniques, compared to the existing Bayesian approaches, and yields state-of-the-art performance.

2 Preliminaries

2.1 Problem statement

Consider an ensemble to be parameterized by a set of functions $Z = \{z_m\}_{m=1}^M \subset V \subset \mathcal{F}$, where V is a ground set, $\mathcal{F}$ is a class of continuous functions, and $z_m : \mathbb{R}^d \to \mathbb{R}^c$, with d the dimensionality of the input data, and c the dimensionality of the output. When training ensembles, we generally want to solve the following optimization problem:

$$\min_{Z \subset V, |Z|=M} \mathcal{R}(Z) - \Omega_{\lambda_M}(Z), \tag{1}$$

where $\mathcal{R}(Z) = \frac{1}{N}\sum_{i=1}^N \ell\left(\frac{1}{M}\sum_{m=1}^M z_m(x_i), y_i\right)$ is the empirical risk of the ensemble, $\ell : \mathcal{Y} \times \mathcal{Y} \to \mathbb{R}_+$ is a loss function, $\mathcal{D} = \{x_i, y_i\}_{i=1}^N$ is a training dataset of size N, and $\Omega_{\lambda_M}(Z)$ is some diversity-promoting term, with diversity regularization strength λ_M.

Empirical observations in the earlier works on ensembles (Lakshminarayanan et al., 2017; Wilson & Izmailov, 2020; Fort et al., 2019) have shown that one can simply ignore $\Omega_{\lambda_M}(Z)$ during optimization, and rely on non-convexity of the loss landscape, minimizing the risks of individual ensemble members. From a variational inference (VI) perspective (Zhang et al., 2019), this can be seen as a *mode-seeking* method, that is, the resulting posterior approximation method aims to put mass at the true posterior modes. Notably, it has been shown experimentally that every ensemble member may discover different modes of the posterior distribution in the function space $p(z|\mathcal{D})$ Fort et al. (2019).

Approximation of $p(z|\mathcal{D})$ is the ultimate aim of this paper, and we argue that randomization-based mode-seeking is insufficient to obtain a good quality approximation of $p(z|\mathcal{D})$, as this procedure does not maximize the coverage of the support of the posterior. In contrast, we aim to find an $\Omega_{\lambda_M}(Z)$ such that the posterior coverage is also maximized. Taking a VI perspective again (Zhang et al., 2019), $\Omega_{\lambda_M}(Z)$ needs to enforce that $\min_{Z \in V, |Z|=M} \; R(Z) - \Omega_{\lambda_M}(Z)$ has also *mean-seeking* behavior. That is, the approximation method should aim to cover as much of the true posterior support as possible while still discovering the high density modes.

2.2 A combinatorial view of ensemble construction

Having now defined the main criteria for (1), we highlight that the problem of constructing an ensemble can be seen from a combinatorial point of view. We therefore treat ensemble construction as subset selection from some ground set of functions, and introduce the main notions of submodular analysis, a powerful tool that enables the analysis of the optimization of set functions (Bach, 2013; Fujishige, 2005).

Definition 1 (Submodularity)**.** *A set function $g : 2^V \to \mathbb{R}$, for the power set of a base set V, is submodular if for all $A \subseteq B \subset V$ and $x \in V \setminus B$*

$$g(A \cup \{x\}) - g(A) \geq g(B \cup \{x\}) - g(B). \tag{2}$$

Definition 2 (Supermodularity and modularity)**.** *A set function is called supermodular if its negative is submodular, and modular if it is both submodular and supermodular.*

Consider now problem (1). Assuming that the loss function ℓ is convex, we can derive an upper-bound on the risk $\mathcal{R}(Z)$ using Jensen's inequality, and obtain a method, which generalizes DE

$$\min_{Z \subset V, |Z|=M} \frac{1}{M}\sum_{m=1}^M \mathcal{R}(z_m) - \Omega_{\lambda_M}(Z), \tag{3}$$

where V is a ground set. In the context of neural networks, it is reasonable to consider the ground set V containing all possible neural networks with a specific architecture and realizable in a computer.

If M is fixed during optimization, $\frac{1}{M}\sum_{m=1}^M \mathcal{R}(z_m)$ contributes a positive modular term to the overall objective. Adding a positive modular function to any set function does not change its submodularity or supermodularity, thus we focus on $\Omega_{\lambda_M}(Z)$. A trivial approach would be to enforce pair-wise diversity by computing a norm of the pairwise differences between functions, i.e. setting $\Omega_{\lambda_M}(Z) = \lambda_M \sum_{i \neq j} \|z_i - z_j\|_*^2$. However, this is a cardinality-fixed submodular *minimization* problem. It is known that it is strongly NP-hard, i.e. there exists no general polynomial time approximation algorithm for it (Svitkina & Fleischer, 2011). The poor quality approximation of this approach is highlighted in Figure 1. We therefore conclude that the choice of $\Omega_{\lambda_M}(Z)$ has a direct impact on the approximabilty of the objective.

3 Submodular analysis of f-divergences

3.1 f-divergences are supermodular functions

Main result. We now consider the problem of approximating a Bayesian posterior via minimization of an f-divergence. Here, we specifically aim our optimization procedure to have both mode and mean-seeking behaviors, i.e. cover the posterior distribution as much as possible, ending up in its mode. We furthermore aim to obtain a polynomial time algorithm that yields a good quality approximation guarantee. In this paper, we leverage classic definitions of approximation algorithm and approximation guarantees.

Definition 3 (Approximation algorithm and guarantees (Williamson & Shmoys, 2011))**.** *A γ-approximation algorithm for an optimization problem is a polynomial-time algorithm that for all instances of the problem produces a solution whose value is within a factor γ of the optimal solution. γ in this case is called approximation guarantee.*

Let us now formally introduce f-divergences.

Definition 4 (f-divergence)**.** *Let $f : \mathbb{R}^+ \to \mathbb{R}$ be a convex function such that $f(1) = 0$, P_z and Q_z be distributions on a measurable space $(\Omega, \mathcal{Z})$ admitting densities $p(z)$ and $q(z)$ with respect to a base measure dz. If P_z is absolutely continuous with respect to Q_z, f-divergence between P_z and $Q_z$is defined as*

$$D_f(P_z||Q_z) = \int_{\mathcal{Z}} f\left(\frac{p(z)}{q(z)}\right) q(z)dz. \tag{4}$$

Consider some density $p(z)$ over continuous functions. We define $q_M(z) = \frac{1}{M}\sum_{m=1}^{M} K(z, z_m)$, where $K_m(z) := K(z, z_m)$ is a kernel centered at z_m used in the density estimation of $p(z)$. In addition, we simplify our notation, always assuming the existence of a measurable space $(\Omega, \mathcal{Z})$ and the base measure dz.

Theorem 1. *Any f-divergence*

$$D_f(p||q_M) = \int f\left(\frac{p(z)}{\frac{1}{M}\sum_{j=1}^{M} K_j(z)}\right) \frac{1}{M}\sum_{m=1}^{M} K_m(z)dz \tag{5}$$

between a distribution $p(z)$ and a normalized mixture of M kernels with equal weights is supermodualar in a cardinality-fixed setting, assuming that $\max_{q_M} D_f(p(z)||q_M(z)) < \infty$.

Proof. The proof is shown in Appendix A.1. □

For some fixed $p(z)$, minimization of (5) with respect to $q_M(z)$ is equivalent to a cardinality-constrained maximization of a non-monotone submodular function of $Z = \{z_1, \dots, z_M\}$. Approximation guarantees for problems of this form are given for non-negative submodular functions (Buchbinder et al., 2014).

One can convert (5) to a non-negative function by defining:

$$F(Z) := -D_f(p||q_M) + C, \tag{6}$$

where $C = \max_{Z \subset V} D_f(p||q_M)$ is a pre-defined constant, which is important for understanding approximation guarantees, but does not need to be computed in practice. After the described transformation, which leads to (6), we obtain $F(Z)$, a *non-negative non-monotone* submodular function.

Approximation guarantees for f-divergences. In the context of submodular functions, there exists an inapproximability result, obtained in (Gharan & Vondrák, 2011), which states that no general polynomial time algorithm with guarantees better than 0.491 exists to solve a submodular maximization problem with constrained cardinality. We note that in practice, however, it might still be possible to obtain a better approximation factor than 0.491 for some specific types of divergences, as these guarantees are defined for *all instances* of the optimization problem (Definition 3).

Let us consider the approximation guarantees for (6), denoting by q_M^* the optimal solution, and by $\hat{q}_M$ a solution found by some algorithm. For an approximation factor γ, we have

$$-D_f(p||\hat{q}_M) + C \geq \gamma(-D_f(p||q_M^*) + C). \tag{7}$$

Simple algebra shows that this implies

$$D_f(p||\hat{q}_M) \leq \gamma \min_{q_M \in A} D_f(p||q_M) + (1-\gamma) \max_{q_M \in A} D_f(p||q_M), \tag{8}$$

where A is a set of possible approximating mixture distributions of size M constructed from the ground set. The derived result indicates that the upper bound on the approximate solution found by minimizing an f-divergence can be substantially dominated by $(1-\gamma)\max_{q_M \in A} D_f(p||q_M)$ if the ground set V is chosen poorly.

3.2 Greedy minimization of f-divergences

Random greedy algorithm. Although submodular optimization has natural parallel extensions and associated approximation guarantees, due to the simplicity of presentation, we focus in this paper on forward greedy selection and use Algorithm 1 for optimizing submodular functions. This algorithm has approximation guarantee of $1/e$ in general Buchbinder et al. (2014). The only required step for this greedy algorithm is a computation of the marginal gain on the objective function $F(Z)$, i.e. $\Delta(z_k|Z) = F(Z \cup \{z_k\}) - F(Z)$.

Algorithm 1 Random Greedy algorithm

Input: V – Ground set
Input: F – Arbitrary submodular function
Input: M – Cardinality of the solution
$Z \leftarrow \emptyset$
for $m = 1$ **to** M **do**
  $R \leftarrow \arg\max_{T \subset V \setminus Z : |T| = M} \sum_{z' \in T} \Delta(z'|Z)$
  $u_i \leftarrow \text{Uniform}(R)$
  $Z \leftarrow Z \cup \{u_i\}$
end for
return Z

Marginal gain. At each step of a greedy algorithm, a marginal gain $\Delta(z_k|Z) = F(Z \cup \{z_k\}) - F(Z)$ of adding a new element z_k to an existing mixture $\sum_{j=1}^{k-1} K_j(z)$ is maximized. For f-divergences, we thus formulate the following proposition:

Proposition 1. *Consider $C = \max D_f(p||q_M)$, where $D_f(p||q_M)$ is an arbitrary f-divergence between some distribution $p(z)$ and a mixture of kernels $q_M(z) = \frac{1}{M}\sum_{j=1}^{M} K_j(z)$, and $D_f(p||q_M) < \infty$. Then, maximization of the marginal gain for the set function*

$$F(Z) = -\int f\left(\frac{p(z)}{\frac{1}{M}\sum_{j=1}^{M} K_j(z)}\right) \frac{1}{M}\sum_{m=1}^{M} K_m(z) dz + C, \tag{9}$$

at step k of a greedy algorithm corresponds to

$$\arg\max_{z_k} \Delta(z_k|Z) = \arg\min_{z_k} \mathbb{E}_{z \sim K_k(z)} f\left(\frac{p(z)}{\frac{1}{M}\sum_{j=1}^{k} K_j(z)}\right). \tag{10}$$

Proof. The proof is shown in Appendix A.2. □

The case of reverse KL divergence. Having mean-seeking behavior is useful to fit the kernel density estimator using *forward* divergences. However, if one wants to optimize marginal gains, they need to have a mode-seeking behavior, which is achieved via optimizing *reverse* divergences (Zhang et al., 2019).

If we consider the generator for the reverse KL-divergence, $f(x) = -\log x$, the minimization becomes

$$\min_{z_k} \mathbb{E}_{z \sim K_k(z)} - \log p(z) + \log\left(\frac{1}{M}\sum_{j=1}^{k} K_j(z)\right). \tag{11}$$

We note that it is costly or even intractable to compute the expectation in (11), and we thus resort to the mean-field assumption. Specifically,

$$p(z) = p(z_1, \ldots, z_M) = \prod_{m=1}^{M} p(z_m), \tag{12}$$

where z_m are variables that partition $p(z)$. In the case of arbitrary multimodal distributions with finite number of modes, such an assumption is well-justified, and also leads to a computationally tractable optimization procedure. Having this assumption in mind, we obtain the following point estimate of (11):

$$\min_{z_k} -\log p(z_k) + \log \left(\frac{1}{M} \sum_{j=1}^{k-1} K_j(z_k) \right). \tag{13}$$

4 Greedy approximation of Bayesian posterior for parametric functions

4.1 Objective function

Derivation of the marginal gain In this section, we consider parametric continuous functions $z_\theta : \mathbb{R}^d \to \mathbb{R}^c$, where d – dimension of the input space, c – dimension of the output space, and θ denotes the parameters determining the function. While our derivations in this section hold for any measurable function that satisfies this definition, we assume a DNN to be our model of choice. For DNNs it is natural to consider a ground set V to be a set of all neural networks with a fixed architecture and a random initialization scheme realizable on a computer. We note that this is a very large, but finite set when considering fixed precision weights.

We now use Bayes' theorem and a mean-field approximation, similarly to (13). This allows us to express the multimodal posterior over a neural network by a product of posteriors of individual ensemble members. Specifically, the factorized posterior is expressed as

$$p(z_\theta|\mathcal{D}) \propto p(z_{\theta_1}, \ldots, z_{\theta_M}|\mathcal{D}) \propto \prod_{m=1}^{M} p(\mathcal{D}|z_{\theta_m}) p(z_{\theta_m}), \tag{14}$$

where θ_m are parameters, $p(\mathcal{D}|z_\theta)$ the likelihood and $p(z_\theta)$ the prior; $p(\mathcal{D}|z_\theta) \propto \prod_{i=1}^{n} \exp(-\ell(z_\theta(x_i), y_i))$, and $p(z_\theta) \propto \exp(-\lambda \|\theta\|_2^2)$.

To leverage our earlier defined submodular maximization machinery, and optimize negative marginal gains derived in (13) for approximating (14), we define the kernel density components via generalized exponential kernels $K_j(z_\theta) \propto \exp(-\lambda_M d(z_\theta, z_{\theta_j})^2)$, where λ_M is proportional to the kernel width and $d(\cdot, \cdot)$ is a distance measure between functions. Substituting the defined kernels and the factorized posterior defined in (14) into (13), we obtain the following objective to minimize at the kth greedy step of Algorithm 1:

$$J(\theta_k) = \underbrace{\mathbb{E}_{(x,y)\sim p(x,y)} \ell(z_{\theta_k}(x), y) + \lambda \|\theta_k\|_2^2}_{\text{Negative marginal gain on } \mathcal{R}(Z)} + \underbrace{\log \sum_{j=1}^{k-1} \exp\left(-\frac{\lambda_M}{M} d(z_{\theta_k}, z_{\theta_j})^2 \right)}_{\text{Negative marginal gain on } \Omega_{\lambda_M}(Z)}, \tag{15}$$

which is similar to the negative marginal gain on our originally defined high-level ensemble training objective (1), except that the diversity term Ω has a different form based on our submodular f-divergence optimization.

Sampling-based approximation of the diversity term. When minimizing (15), one needs to be able to compute the diversity term $\Omega = \log \sum_{j=1}^{k-1} \exp(-\lambda_M d(z_\theta, z_{\theta_j})^2)$, which is derived from a kernel density estimator we aim to fit to the true posterior. We note that this needs to be done *in the function space*, which makes this computation non-trivial.

We earlier defined $K_j(z)$ to be an individual kernel in a mixture $\frac{1}{M} \sum_{j=1}^{M} K_j(z)$. In order to be able to use the f-divergence, the individual components $K_j(z)$ must be density functions centered at z_j, which implies the need of a notion of similarity or the existence of a function norm, which are known to be NP-hard to compute for neural networks

with depth greater than 3 (Rannen-Triki et al., 2019). We note that this intrinsic hardness result applies to *all* methods that define a meaningful posterior distribution in function space through a kernel density estimator. We thus use here a method from (Rannen-Triki et al., 2019) to approximate $\|z\|_2^2$, via i.i.d. samples $x_i \sim P^*$, where P^* is a weighting distribution, which is required to ensure that Monte Carlo integration yields a reasonable approximation. This leads to the following sampling-based approximation of the diversity term:

$$\log \sum_{j=1}^{k-1} \exp\left(-\frac{\lambda_M}{M} \mathbb{E}_{x\sim p^*(x)} \|z_{\theta_k}(x) - z_{\theta_j}(x)\|_2^2\right). \tag{16}$$

4.2 Practical implementation

Computing the diversity term To this point, we defined all the main components of our method, except the weighting distribution in (16). The desirable behavior, which we expect an ensemble to exhibit, is that it must be uncertain on the OOD data and certain in the regions where the training data are available. This implies that $p^*(x)$ *must include* OOD samples. One can use OOD data in training explicitly, however, in our work, resort to a setting when OOD data are unknown. Specifically, we use a simple heuristic, which fits a Gaussian to every data dimension with the variance $\times 5$ larger than the variance of the data. We specify further details about this in Appendix B.1.

The resulting algorithm The resulting, computationally tractable optimization algorithm for ensembles, which minimizes negative marginal gains (10), is shown in Algorithm 2. For simplicity, we omit the snapshot selection step, i.e. early stopping.

We note that in Algorithm 1 line 7 we require a uniform random sampling over the top M functions. In practice on a computer, the set of functions are parameterized by fixed precision floating point numbers, and that there are a large number of functions differing by a single lowest significant bit of one network weight, effectively achieving the same value of the negative marginal gain up to measurement error (recall the NP-hardness of the diversity term and its approximation by Monte Carlo integration). Therefore, the randomization introduced by Algorithm 1 line 7 is lower than the combination of optimization error and approximation error from Monte Carlo integration. There is therefore no gain from performing multiple optimizations and we replace the uniform random selection step with a single stochastic optimization: At each kth greedy step, we change the seed (`set_seed`$(\cdot)$ in Algorithm 2) of the random number generator before initializing the model and optimize a neural network using stochastic gradient descent from random initialization. The final computational performance improvement can be obtained by storing the evaluations $z_j(x_i)\ \forall j = 1, \ldots, k-1$ in memory before executing each kth step.

We report here also one practical trick, which we found important during training. Specifically, freezing the batch normalization layers (Ioffe & Szegedy, 2015) before computing the diversity term turned out to help the convergence substantially.

Algorithm 2 $\mathcal{O}(k)$ Random Greedy algorithm for training ensembles of neural networks. `set_seed`$(\cdot)$ sets the random seed. The $\arg\min_\theta$ on line 10 is achieved by stochastic gradient descent with random weight initialization.

1: **Input:** V – Set of all neural networks specified by some architecture
2: **Input:** M – Cardinality of the solution
3: **Input:** $p(x, y)$ – Training data / empirical distribution
4: **Input:** $p^*(x)$ – Weighting distribution for the diversity term
5: **Input:** s – Initial random seed
6: $\theta_1 \leftarrow \arg\min_{\theta_m} \mathbb{E}_{(x,y)\sim p(x,y)} \ell(z_{\theta_1}(x), y) + \lambda \|\theta_1\|_2^2$
7: $Z \leftarrow \{z_{\theta_1}\}$
8: **for** $m = 2$ **to** M **do**
9: `set_seed`$(s + m - 1)$;
10: $\theta_m \leftarrow \arg\min_\theta \mathbb{E}_{(x,y)} \ell(z_\theta(x), y) + \lambda \|\theta\|_2^2 + \log \sum_{j=1}^{m-1} \exp\left(-\frac{\lambda_M}{M} \mathbb{E}_{x^*\sim p^*(x)} \|z_\theta(x^*) - z_{\theta_j}(x^*)\|_2^2\right)$
11: $Z \leftarrow Z \cup \{z_{\theta_m}\}$;
12: **end for**
13: **return** Z

5 Related work

Randomization-based ensembles. Generally, ensembles have been studied in Machine Learning over several decades for different classes of models (Hansen & Salamon, 1990; Breiman, 1996; Freund & Schapire, 1997; Lakshminarayanan et al., 2017). One can distinguish several main methods for diverse ensemble construction (Pearce et al., 2020): randomization of training initialization and hyperparameters (Hansen & Salamon, 1990; Wenzel et al., 2020b; Wilson & Izmailov, 2020; Zaidi et al., 2020), bagging (Breiman, 1996; 2001), boosting (Freund & Schapire, 1997), and explicit diversity training (Kuncheva & Whitaker, 2003; Ross et al., 2020; Yang et al., 2020; Brown et al., 2005; Kariyappa & Qureshi, 2019; Sinha et al., 2020; Melville & Mooney, 2005). Randomization-based ensemble construction has shown good results in in-domain uncertainty (Ashukha et al., 2020) estimation, but also in the detection of OOD data (Lakshminarayanan et al., 2017).

Submodular ensemble pruning and greedy ensemble construction Submodularity in ensemble learning has previously been discussed in the context of ensemble pruning (Sha et al., 2014). The goal of ensemble pruning is to trim a large ensemble of models so that the accuracy of the ensemble remains the same. We note that recently, inspired by the submodular pruning approach, a greedy algorithm has been applied to randomization based ensembles (Wenzel et al., 2020b; Zaidi et al., 2020). However, we also note that neither of these works approached the problem of ensemble construction from a Bayesian posterior approximation point of view. However, they provide extensive experimental evidence on the plausibility of greedy approach. Our work sheds light on *why* in Wenzel et al. (2020b); Zaidi et al. (2020) ensembles constructed greedily worked well in OOD detection tasks.

Diversity-promoting regularization for ensemble training. The ensemble literature contains a line of work focusing on explicitly promoting regularization in ensembles (Kuncheva & Whitaker, 2003; Ross et al., 2020; Yang et al., 2020; Brown et al., 2005; Kariyappa & Qureshi, 2019; Sinha et al., 2020; Melville & Mooney, 2005; Havasi et al., 2021). In terms of promoting diversity outside training data, the closest work to ours is (Ross et al., 2020; Rame & Cord, 2021), and in terms of the form of diversity regularization it is (Kariyappa & Qureshi, 2019). However, none of these works takes the perspective of approximating the Bayesian posterior. Another limitation of most of these approaches is that they use either out-of-distribution data in training, adversarial examples, or expensive generative models, thus making those methods difficult to scale to large datasets.

POVI A problem of learning diverse ensembles can be seen from a POVI perspective: in particular, Stein Variational Gradient Descent (SVGD) (Wang & Liu, 2019). SVGD aims to learn a diverse set of functions Z, approximating arbitrary distributions via a set of particles using a reverse KL divergence. This approach is similar to ours, however, we tackle the problem of optimizing a *general f-divergence* in the function space. Furthermore, to our knowledge, the present work is the first that takes a submodular minimization perspective in BDL.

Another line of work in the POVI family also considers greedy approximations (Futami et al., 2019; Jerfel et al., 2021). In both of these works, the authors perform particle based inference by also optimizing the kernel widths of the KDE, which is different to our method. Furthermore, these works do not tell what the diversity term for ensemble training should look like, and how to compute it in practice.

Function space POVI Conventionally, Bayesian inference in DL is thought of in the weight space (MacKay, 1992; Blundell et al., 2015; Gal & Ghahramani, 2016; Izmailov et al., 2020; Wilson & Izmailov, 2020; Pearce et al., 2020; Wenzel et al., 2020a). However, recent studies point out that despite the fact that simple priors over weights may imply complex posteriors in the function space, the connection between two of these is difficult to establish (Sun et al., 2019; Hafner et al., 2020).

Recent papers on function-space POVI (Wang et al., 2019; D'Angelo & Fortuin, 2021) point out that one can do Bayesian inference in the function space by optimizing an objective function with a repulsive term. Notably, they draw connection to the reverse KL-divergence minimization, and we thus consider our method to be closely connected to function space POVI.

6 Experiments

6.1 Setup

Datasets and models. We ran our main experiments on CIFAR10, CIFAR100 (Krizhevsky, 2009) and SVHN (Netzer et al., 2011) in-distribution datasets. Our OOD detection benchmark included CIFAR10, CIFAR100, DTD (Cimpoi et al., 2014), SVHN (Netzer et al., 2011), LSUN (Yu et al., 2015), TinyImageNet (Le & Yang, 2015), Places 365 (Zhou et al., 2017), Bernoulli noise images, Gaussian noise, random blobs image, and uniform noise images. The composition of the benchmark was inspired by the work of Hendrycks et al. (2018). We excluded the in-distribution datasets for each of the settings, resulting in a total of 10 OOD datasets for each in-distribution dataset. The full description of the benchmark is shown in Appendix B.2.

The experiments were conducted using ResNet164 (pre-activated version; denoted as PreResNet164) (He et al., 2016), VGG16 (with batch normalization (Ioffe & Szegedy, 2015); denoted as VGG16BN) (Simonyan & Zisserman, 2015), and WideResNet28x10 (Zagoruyko & Komodakis, 2016). All our models in the ensembles were trained for 100 epochs using PyTorch (Paszke et al., 2019), each ensemble on a single NVIDIA V100 GPU. In the case of CIFAR and SVHN experiments, we trained ensembles of size $M = 11$, and report the results across 5 different random seeds. For the CIFAR experiments, we selected $\lambda_M \in \{0.001, 0.005, 0.01, 0.05, 0.1, 0.5, 1, 3, 5, 7, 10\}$. In addition to the CIFAR and SVHN experiments, we used MNIST (LeCun et al., 1998) with ResNet8. The details of those experiments are shown in Appendix B.2.

Model selection and metrics. We used mutual information (MI) between the distribution of the predicted label $\hat{y}$ for the point $\hat{\mathbf{x}}$ and the posterior distribution over functions $p(f|\mathcal{D})$, to evaluate the *epistemic uncertainty* (Malinin & Gales, 2018; Depeweg et al., 2018) and reported the area under the ROC curve (AUC) and area under the precision-recall (PR) curve, i.e. average precision (AP) to quantify the OOD detection performance. Furthermore, we computed the false positive rate at 95% true positive rate (FPR95). Details on the computation of epistemic uncertainty can be found in Appendix B.3.

6.2 Results

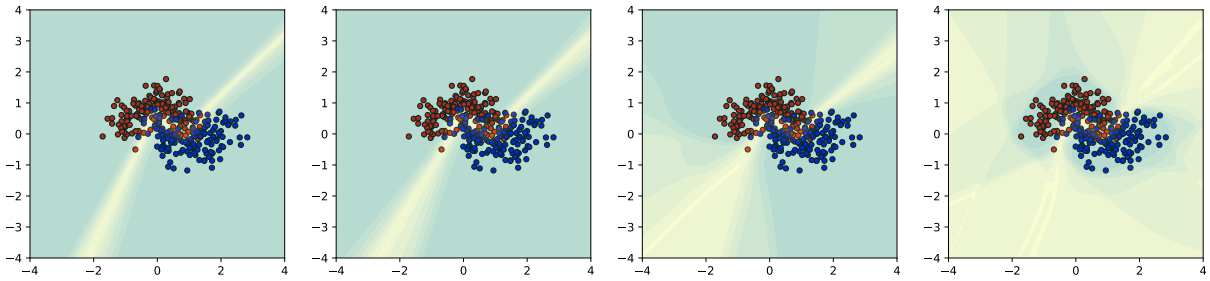

(a) Deep Ensembles (b) $\lambda_M = 0.1$ (c) $\lambda_M = 1$ (d) $\lambda_M = 10$

Figure 2: Uncertainty of an ensemble of two layer neural networks on a two moons dataset (size $M = 11$). Compared to DE, which is uncertain only close to the decision boundary, our method yields the desired behavior – the further we move from training data, the higher uncertainty is. Such behavior is controlled by the diversity regularization coefficient λ_M.

Illustrative examples. Figure 2 illustrates how our method performs on the two moons dataset. Here, we used a two-layer fully-connected network with ReLU activations (Fukushima, 1988). Having a high λ_M is important to obtain good uncertainty estimation. As expected, compared to our method, the DE method does not explicitly maximize the coverage of the posterior, and thus fails to be uncertain outside the training data.

Out-of-distribution detection. We present aggregated results for all the models and in-distribution datasets in Table 1. It is clear that on average (across OOD datasets), our method is substantially better than DE. This holds for all the architectures and in-distribution datasets. We show the expanded version of all the OOD detection results

in Appendix C.3. An example of these results is shown in Figure 3 for all the models trained on CIFAR 100. Here, one can see that our method is at least similar to DE, and substantially better overall in terms of AUC and AP metrics. Finally, some examples of OOD detection by both DE and our method are shown in Figure 4. Here, we computed optimal thresholds for each of the methods by optimizing the trade-off between the true positive and true negative rates.

Table 1: Averaged metrics across 10 OOD datasets.

Model	**Dataset**	**Deep Ensembles**			**Ours**		
		AUC (↑)	**AP (↑)**	**FPR95 (↓)**	**AUC (↑)**	**AP (↑)**	**FPR95 (↓)**
PreResNet164	C10	0.94	0.92	0.17	**0.95**	**0.95**	**0.14**
	C100	0.79	0.80	0.47	**0.88**	**0.88**	**0.40**
	SVHN	0.99	0.97	0.02	**1.00**	**0.98**	**0.01**
WideResNet28x10	C10	0.95	0.94	0.15	**0.96**	**0.96**	**0.12**
	C100	0.86	0.85	0.36	**0.90**	**0.91**	**0.30**
	SVHN	0.99	0.96	0.03	**1.00**	**0.99**	**0.01**
VGG16BN	C10	0.92	0.91	0.23	**0.95**	**0.95**	**0.18**
	C100	0.83	0.82	0.45	**0.89**	**0.90**	**0.36**
	SVHN	0.99	0.96	0.02	**1.00**	**0.98**	0.02

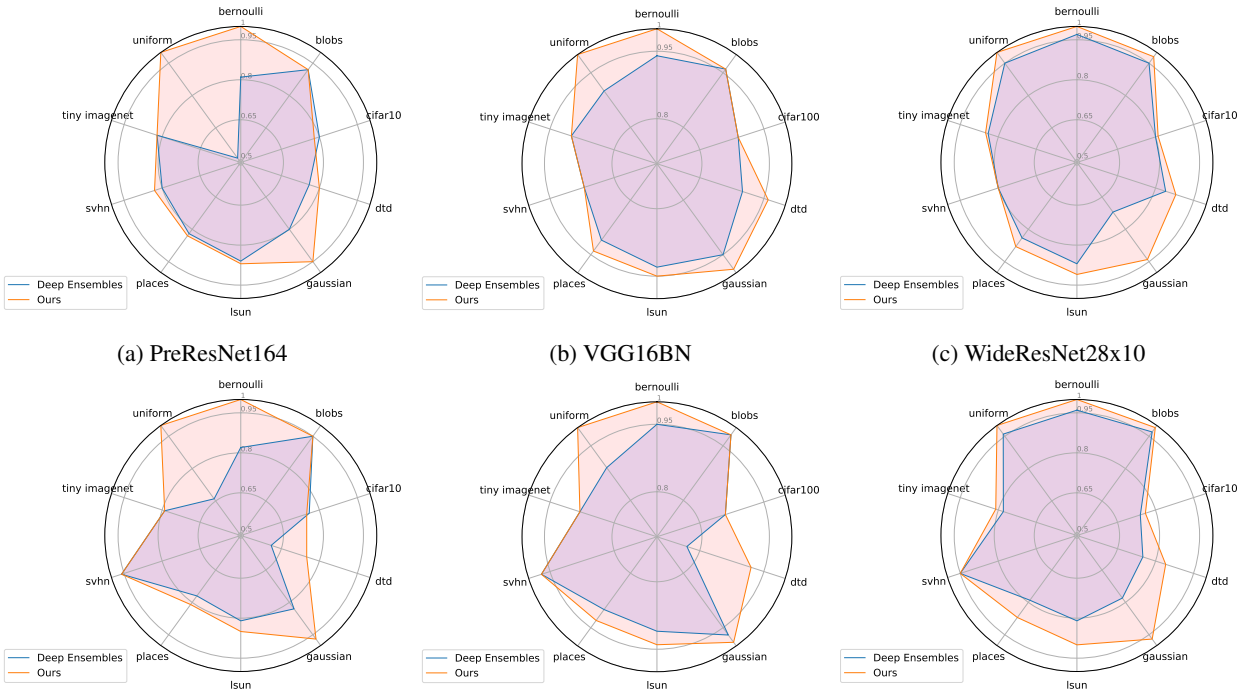

(a) PreResNet164 (b) VGG16BN (c) WideResNet28x10

(d) PreResNet164 (e) VGG16BN (f) WideResNet28x10

Figure 3: Out-of distribution detection results on CIFAR 100 for 3 different architectures (read column-wise). Here, we show AUC (top row) and AP values (bottom row) from 0.5 to 1 averaged across 5 seeds.

7 Discussion

In this paper, we have introduced a novel paradigm for Bayesian posterior approximation in Deep Learning using greedy ensemble construction via submodular optimization. We have proven a new general theoretical result, which shows that minimization of an f-divergence between some distribution and a kernel density estimator has approximation

(a) (b)

Figure 4: OOD detection examples. In subplot (a), the top row shows true positives, and the bottom – true negatives detected by our method. We also show the uncertainty values. Subplot (b) shows the failures of both DE and our method on positives (top row) and negatives (bottom row), respectively. Here, we used PreResNet164 trained on CIFAR10 ($M = 11$). SVHN was used as an OOD dataset.

guarantees, and can be done greedily. We then derived a novel coverage promoting diversity term for ensemble construction. The results presented in this paper, as well as in Appendix C.4, demonstrate that our method outperforms the state-of-the-art approach for ensemble construction, DE (Lakshminarayanan et al., 2017), on a range of benchmarks in OOD detection, while preserving the accuracy (Table C3).

This study has some limitations, which outline several directions for the future work. Firstly, we did not compare our approach to a variety of existing methods for ensemble generation, e.g. snapshot ensembles (Huang et al., 2017), batch ensembles (Wen et al., 2020) or hyperparameter ensembles (Wenzel et al., 2020b). However, these methods are heuristic, and as discussed in the related work, our method can be used in conjunction with them to make them more principled. Furthermore, we note that the main contribution of this paper is novel theory.

The second limitation of this work is that it does not compare to f-POVI Wang et al. (2019); D'Angelo & Fortuin (2021). However, as noted earlier, those methods are in a different class, as they focus on training models without state-of-the-art training techniques such as batch normalization (Ioffe & Szegedy, 2015) and data augmentation.

The third limitation is that we did not fully explore different techniques of generating weighting distributions for the diversity term. However, we still evaluated the possibility of using real images for this purpose in Appendix C.4, similarly to an outlier exposure setting (Hendrycks et al., 2018).

The final limitation is related to our method, as it lacks parallelization possibilities compared to DE. We note, however, that there is a class of parallel submodular optimization algorithms that enable parallelization and retain approximation guarantees (Ene & Nguyen, 2020). When both our method and DE are run sequentially on GPU, one can observe 70-90% computational overhead compared to DE when running our method for $M = 11$ (Table C9). Such an overhead, is, however, natural due to saving predictions and a double number of forward passes. We note here, that despite that training of the proposed method was roughly 1.75-1.9 times more expensive than DE, both methods had the same test runtime. Therefore, our approach is still of interest in applications where high quality uncertainty estimation at test time cannot be traded in favor of lower cost training.

To conclude, this paper provides a novel foundational framework for Bayesian Deep Learning. We hope for the wide adaption of the proposed method by practitioners across the fields. Our code is available at `https://anonymous.4open.science/r/greedy_ensembles_training-0CD6/`.

References

Arsenii Ashukha, Alexander Lyzhov, Dmitry Molchanov, and Dmitry Vetrov. Pitfalls of in-domain uncertainty estimation and ensembling in deep learning. *arXiv preprint arXiv:2002.06470*, 2020.

Francis Bach. Learning with submodular functions: A convex optimization perspective. *Foundations and Trends in Machine Learning*, 6(2-3):145–373, 2013.

Francis Bach. Submodular functions: from discrete to continuous domains. *Mathematical Programming*, 175(1): 419–459, 2019.

Charles Blundell, Julien Cornebise, Koray Kavukcuoglu, and Daan Wierstra. Weight uncertainty in neural network. In *International Conference on Machine Learning*, pp. 1613–1622. PMLR, 2015.

Leo Breiman. Bagging predictors. *Machine learning*, 24(2):123–140, 1996.

Leo Breiman. Random forests. *Machine learning*, 45(1):5–32, 2001.

Gavin Brown, Jeremy L Wyatt, Peter Tino, and Yoshua Bengio. Managing diversity in regression ensembles. *Journal of machine learning research*, 6(9), 2005.

Niv Buchbinder, Moran Feldman, Joseph Naor, and Roy Schwartz. Submodular maximization with cardinality constraints. In *Proceedings of the twenty-fifth annual ACM-SIAM symposium on Discrete algorithms*, pp. 1433–1452. SIAM, 2014.

Mircea Cimpoi, Subhransu Maji, Iasonas Kokkinos, Sammy Mohamed, and Andrea Vedaldi. Describing textures in the wild. In *Proceedings of the IEEE Conference on Computer Vision and Pattern Recognition*, pp. 3606–3613, 2014.

Kamil Ciosek, Vincent Fortuin, Ryota Tomioka, Katja Hofmann, and Richard Turner. Conservative uncertainty estimation by fitting prior networks. In *International Conference on Learning Representations*, 2019.

Francesco D'Angelo and Vincent Fortuin. Repulsive deep ensembles are bayesian. *Advances in Neural Information Processing Systems*, 34, 2021.

Jia Deng, Wei Dong, Richard Socher, Li-Jia Li, Kai Li, and Li Fei-Fei. Imagenet: A large-scale hierarchical image database. In *2009 IEEE conference on computer vision and pattern recognition*, pp. 248–255. Ieee, 2009.

Stefan Depeweg, Jose-Miguel Hernandez-Lobato, Finale Doshi-Velez, and Steffen Udluft. Decomposition of uncertainty in bayesian deep learning for efficient and risk-sensitive learning. In *International Conference on Machine Learning*, pp. 1184–1193. PMLR, 2018.

Alina Ene and Huy Nguyen. Parallel algorithm for non-monotone dr-submodular maximization. In *International Conference on Machine Learning*, pp. 2902–2911. PMLR, 2020.

Stanislav Fort, Huiyi Hu, and Balaji Lakshminarayanan. Deep ensembles: A loss landscape perspective. *arXiv preprint arXiv:1912.02757*, 2019.

Vincent Fortuin. Priors in bayesian deep learning: A review. *arXiv preprint arXiv:2105.06868*, 2021.

Yoav Freund and Robert E Schapire. A decision-theoretic generalization of on-line learning and an application to boosting. *Journal of computer and system sciences*, 55(1):119–139, 1997.

Satoru Fujishige. *Submodular functions and optimization*. Elsevier, 2005.

Kunihiko Fukushima. Neocognitron: A hierarchical neural network capable of visual pattern recognition. *Neural networks*, 1(2):119–130, 1988.

Futoshi Futami, Zhenghang Cui, Issei Sato, and Masashi Sugiyama. Bayesian posterior approximation via greedy particle optimization. In *Proceedings of the AAAI Conference on Artificial Intelligence*, volume 33, pp. 3606–3613, 2019.

Yarin Gal. *Uncertainty in Deep Learning*. PhD thesis, University of Cambridge, 2016.

Yarin Gal and Zoubin Ghahramani. Dropout as a Bayesian approximation: Representing model uncertainty in deep learning. In *international conference on machine learning*, pp. 1050–1059. PMLR, 2016.

Timur Garipov, Pavel Izmailov, Dmitrii Podoprikhin, Dmitry Vetrov, and Andrew Gordon Wilson. Loss surfaces, mode connectivity, and fast ensembling of DNNs. In *Proceedings of the 32nd International Conference on Neural Information Processing Systems*, pp. 8803–8812, 2018.

Shayan Oveis Gharan and Jan Vondrák. Submodular maximization by simulated annealing. In *Proceedings of the twenty-second annual ACM-SIAM symposium on Discrete Algorithms*, pp. 1098–1116. SIAM, 2011.

Danijar Hafner, Dustin Tran, Timothy Lillicrap, Alex Irpan, and James Davidson. Noise contrastive priors for functional uncertainty. In *Uncertainty in Artificial Intelligence*, pp. 905–914. PMLR, 2020.

Lars Kai Hansen and Peter Salamon. Neural network ensembles. *IEEE transactions on pattern analysis and machine intelligence*, 12(10):993–1001, 1990.

Marton Havasi, Rodolphe Jenatton, Stanislav Fort, Jeremiah Zhe Liu, Jasper Snoek, Balaji Lakshminarayanan, Andrew Mingbo Dai, and Dustin Tran. Training independent subnetworks for robust prediction. In *International Conference on Learning Representations*, 2021. URL `https://openreview.net/forum?id=OGg9XnKxFAH`.

Bobby He, Balaji Lakshminarayanan, and Yee Whye Teh. Bayesian deep ensembles via the neural tangent kernel. *Advances in Neural Information Processing Systems*, 33:1010–1022, 2020.

Kaiming He, Xiangyu Zhang, Shaoqing Ren, and Jian Sun. Identity mappings in deep residual networks. In *European conference on computer vision*, pp. 630–645. Springer, 2016.

Dan Hendrycks and Thomas Dietterich. Benchmarking neural network robustness to common corruptions and perturbations. *arXiv preprint arXiv:1903.12261*, 2019.

Dan Hendrycks, Mantas Mazeika, and Thomas Dietterich. Deep anomaly detection with outlier exposure. *arXiv preprint arXiv:1812.04606*, 2018.

Gao Huang, Yixuan Li, Geoff Pleiss, Zhuang Liu, John E Hopcroft, and Kilian Q Weinberger. Snapshot ensembles: Train 1, get m for free. *arXiv preprint arXiv:1704.00109*, 2017.

Alexander Immer, Matthias Bauer, Vincent Fortuin, Gunnar Rätsch, and Khan Mohammad Emtiyaz. Scalable marginal likelihood estimation for model selection in deep learning. In *International Conference on Machine Learning*, pp. 4563–4573. PMLR, 2021.

Sergey Ioffe and Christian Szegedy. Batch normalization: Accelerating deep network training by reducing internal covariate shift. In *International conference on machine learning*, pp. 448–456. PMLR, 2015.

Pavel Izmailov, Wesley J Maddox, Polina Kirichenko, Timur Garipov, Dmitry Vetrov, and Andrew Gordon Wilson. Subspace inference for Bayesian deep learning. In *Uncertainty in Artificial Intelligence*, pp. 1169–1179. PMLR, 2020.

Ghassen Jerfel, Serena Wang, Clara Fannjiang, Katherine A Heller, Yian Ma, and Michael I Jordan. Variational refinement for importance sampling using the forward Kullback-Leibler divergence. *arXiv preprint arXiv:2106.15980*, 2021.

Sanjay Kariyappa and Moinuddin K Qureshi. Improving adversarial robustness of ensembles with diversity training. *arXiv preprint arXiv:1901.09981*, 2019.

Andreas Krause, Ajit Singh, and Carlos Guestrin. Near-optimal sensor placements in gaussian processes: Theory, efficient algorithms and empirical studies. *Journal of Machine Learning Research*, 9(2), 2008.

Alex Krizhevsky. Learning multiple layers of features from tiny images. Technical report, University of Toronto, 2009.

Ludmila I Kuncheva and Christopher J Whitaker. Measures of diversity in classifier ensembles and their relationship with the ensemble accuracy. *Machine learning*, 51(2):181–207, 2003.

Brenden M Lake, Ruslan Salakhutdinov, and Joshua B Tenenbaum. Human-level concept learning through probabilistic program induction. *Science*, 350(6266):1332–1338, 2015.

Balaji Lakshminarayanan, Alexander Pritzel, and Charles Blundell. Simple and scalable predictive uncertainty estimation using deep ensembles. In *Advances in neural information processing systems*, pp. 6402–6413, 2017.

Ya Le and Xuan Yang. Tiny imagenet visual recognition challenge. CS 231N, Stanford University, 2015.

Yann LeCun, Léon Bottou, Yoshua Bengio, and Patrick Haffner. Gradient-based learning applied to document recognition. *Proceedings of the IEEE*, 86(11):2278–2324, 1998.

Zhiyun Lu, Eugene Ie, and Fei Sha. Uncertainty estimation with infinitesimal jackknife, its distribution and mean-field approximation. *arXiv preprint arXiv:2006.07584*, 2020.

David JC MacKay. A practical bayesian framework for backpropagation networks. *Neural computation*, 4(3):448–472, 1992.

Wesley J Maddox, Pavel Izmailov, Timur Garipov, Dmitry P Vetrov, and Andrew Gordon Wilson. A simple baseline for Bayesian uncertainty in deep learning. In *Advances in Neural Information Processing Systems*, pp. 13132–13143, 2019.

Andrey Malinin and Mark Gales. Predictive uncertainty estimation via prior networks. NIPS'18, pp. 7047–7058, Red Hook, NY, USA, 2018. Curran Associates Inc.

Prem Melville and Raymond J Mooney. Creating diversity in ensembles using artificial data. *Information Fusion*, 6(1): 99–111, 2005.

Dragoslav S Mitrinovic and Petar M Vasic. *Analytic inequalities*, volume 61. Springer, 1970.

Yuval Netzer, Tao Wang, Adam Coates, Alessandro Bissacco, Bo Wu, and Andrew Y Ng. Reading digits in natural images with unsupervised feature learning. 2011.

Jeremy Nixon, Michael W Dusenberry, Linchuan Zhang, Ghassen Jerfel, and Dustin Tran. Measuring calibration in deep learning. In *Proceedings of the IEEE/CVF International Conference on Computer Vision Workshops*, volume 2, 2019.

Yaniv Ovadia, Emily Fertig, Jie Ren, Zachary Nado, David Sculley, Sebastian Nowozin, Joshua V Dillon, Balaji Lakshminarayanan, and Jasper Snoek. Can you trust your model's uncertainty? evaluating predictive uncertainty under dataset shift. *arXiv preprint arXiv:1906.02530*, 2019.

Adam Paszke, Sam Gross, Francisco Massa, Adam Lerer, James Bradbury, Gregory Chanan, Trevor Killeen, Zeming Lin, Natalia Gimelshein, Luca Antiga, et al. Pytorch: An imperative style, high-performance deep learning library. *Advances in Neural Information Processing Systems*, 32:8026–8037, 2019.

Tim Pearce, Felix Leibfried, and Alexandra Brintrup. Uncertainty in neural networks: Approximately Bayesian ensembling. In *International conference on artificial intelligence and statistics*, pp. 234–244. PMLR, 2020.

Fabian Pedregosa, Gaël Varoquaux, Alexandre Gramfort, Vincent Michel, Bertrand Thirion, Olivier Grisel, Mathieu Blondel, Peter Prettenhofer, Ron Weiss, Vincent Dubourg, et al. Scikit-learn: Machine learning in python. *the Journal of machine Learning research*, 12:2825–2830, 2011.

Alexandre Rame and Matthieu Cord. Dice: Diversity in deep ensembles via conditional redundancy adversarial estimation. *arXiv preprint arXiv:2101.05544*, 2021.

Amal Rannen-Triki, Maxim Berman, Vladimir Kolmogorov, and Matthew B Blaschko. Function norms for neural networks. In *Proceedings of the IEEE International Conference on Computer Vision Workshops*, 2019.

Andrew Ross, Weiwei Pan, Leo Celi, and Finale Doshi-Velez. Ensembles of locally independent prediction models. In *Proceedings of the AAAI Conference on Artificial Intelligence*, volume 34, pp. 5527–5536, 2020.

Chaofeng Sha, Keqiang Wang, Xiaoling Wang, and Aoying Zhou. Ensemble pruning: A submodular function maximization perspective. In *International Conference on Database Systems for Advanced Applications*, pp. 1–15. Springer, 2014.

Karen Simonyan and Andrew Zisserman. Very deep convolutional networks for large-scale image recognition. In Yoshua Bengio and Yann LeCun (eds.), *3rd International Conference on Learning Representations, ICLR 2015, San Diego, CA, USA, May 7-9, 2015, Conference Track Proceedings*, 2015. URL `http://arxiv.org/abs/1409.1556`.

Samarth Sinha, Homanga Bharadhwaj, Anirudh Goyal, Hugo Larochelle, Animesh Garg, and Florian Shkurti. Dibs: Diversity inducing information bottleneck in model ensembles. *arXiv preprint arXiv:2003.04514*, 2020.

Leslie N Smith and Nicholay Topin. Super-convergence: Very fast training of neural networks using large learning rates. In *Artificial Intelligence and Machine Learning for Multi-Domain Operations Applications*, volume 11006, pp. 1100612. International Society for Optics and Photonics, 2019.

Shengyang Sun, Guodong Zhang, Jiaxin Shi, and Roger Grosse. Functional variational Bayesian neural networks. *arXiv preprint arXiv:1903.05779*, 2019.

Zoya Svitkina and Lisa Fleischer. Submodular approximation: Sampling-based algorithms and lower bounds. *SIAM Journal on Computing*, 40(6):1715–1737, 2011.

Joost Van Amersfoort, Lewis Smith, Yee Whye Teh, and Yarin Gal. Uncertainty estimation using a single deep deterministic neural network. In *International Conference on Machine Learning*, pp. 9690–9700. PMLR, 2020.

Dilin Wang and Qiang Liu. Nonlinear Stein variational gradient descent for learning diversified mixture models. In *International Conference on Machine Learning*, pp. 6576–6585, 2019.

Ziyu Wang, Tongzheng Ren, Jun Zhu, and Bo Zhang. Function space particle optimization for Bayesian neural networks. *arXiv preprint arXiv:1902.09754*, 2019.

Yeming Wen, Dustin Tran, and Jimmy Ba. Batchensemble: an alternative approach to efficient ensemble and lifelong learning. *arXiv preprint arXiv:2002.06715*, 2020.

Florian Wenzel, Kevin Roth, Bastiaan S Veeling, Jakub Świątkowski, Linh Tran, Stephan Mandt, Jasper Snoek, Tim Salimans, Rodolphe Jenatton, and Sebastian Nowozin. How good is the Bayes posterior in deep neural networks really? *arXiv preprint arXiv:2002.02405*, 2020a.

Florian Wenzel, Jasper Snoek, Dustin Tran, and Rodolphe Jenatton. Hyperparameter ensembles for robustness and uncertainty quantification. In H. Larochelle, M. Ranzato, R. Hadsell, M. F. Balcan, and H. Lin (eds.), *Advances in Neural Information Processing Systems*, volume 33, pp. 6514–6527. Curran Associates, Inc., 2020b.

David P Williamson and David B Shmoys. *The design of approximation algorithms*. Cambridge university press, 2011.

Andrew G Wilson and Pavel Izmailov. Bayesian deep learning and a probabilistic perspective of generalization. *Advances in neural information processing systems*, 33:4697–4708, 2020.

Han Xiao, Kashif Rasul, and Roland Vollgraf. Fashion-mnist: a novel image dataset for benchmarking machine learning algorithms. *arXiv preprint arXiv:1708.07747*, 2017.

Huanrui Yang, Jingyang Zhang, Hongliang Dong, Nathan Inkawhich, Andrew Gardner, Andrew Touchet, Wesley Wilkes, Heath Berry, and Hai Li. Dverge: diversifying vulnerabilities for enhanced robust generation of ensembles. *arXiv preprint arXiv:2009.14720*, 2020.

Fisher Yu, Ari Seff, Yinda Zhang, Shuran Song, Thomas Funkhouser, and Jianxiong Xiao. Lsun: Construction of a large-scale image dataset using deep learning with humans in the loop. *arXiv preprint arXiv:1506.03365*, 2015.

Sergey Zagoruyko and Nikos Komodakis. Wide residual networks. In *British Machine Vision Conference 2016*. British Machine Vision Association, 2016.

Sheheryar Zaidi, Arber Zela, Thomas Elsken, Chris Holmes, Frank Hutter, and Yee Whye Teh. Neural ensemble search for performant and calibrated predictions. *arXiv preprint arXiv:2006.08573*, 2020.

Hongyi Zhang, Moustapha Cisse, Yann N. Dauphin, and David Lopez-Paz. mixup: Beyond empirical risk minimization. In *International Conference on Learning Representations*, 2018. URL `https://openreview.net/forum?id=r1Ddp1-Rb`.

Mingtian Zhang, Thomas Bird, Raza Habib, Tianlin Xu, and David Barber. Variational f-divergence minimization. *arXiv preprint arXiv:1907.11891*, 2019.

Bolei Zhou, Agata Lapedriza, Aditya Khosla, Aude Oliva, and Antonio Torralba. Places: A 10 million image database for scene recognition. *IEEE transactions on pattern analysis and machine intelligence*, 40(6):1452–1464, 2017.

A Proofs

A.1 Proof of Theorem 1

To prove Theorem 1, we make use of the following theorem:

Theorem A1 (Theorem 1.4 from (Mitrinovic & Vasic, 1970))**.** *A function $f : D \to R$ is convex on $D = [a, b]$ if and only if $\forall x_1 < x_2 < x_3 \in D$*

$$\begin{vmatrix} x_1 & f(x_1) & 1 \\ x_2 & f(x_2) & 1 \\ x_3 & f(x_3) & 1 \end{vmatrix} \geq 0. \tag{17}$$

Theorem 1. *Any f-divergence*

$$D_f(p||q_M) = \int f\left(\frac{p(z)}{\frac{1}{M}\sum_{j=1}^{M} K_j(z)}\right)\frac{1}{M}\sum_{m=1}^{M} K_m(z)dz \tag{18}$$

between a distribution $p(z)$ and a mixture of M kernels with equal weights is supermodualar in a cardinality-fixed setting, assuming that $\forall z \max_{q_M} D_f(p(z)||q_M(z)) < \infty$.

Proof. In order to prove that f-divergences are supermodular, we need to show that $\forall \alpha > 0$, $xf(\frac{\alpha}{x})$ is convex, because $q_M(z)$ is a positive modular function (Bach, 2019, Proposition 6.1), due to M being fixed.

From Theorem A1, $f(x)$ is convex on a closed interval $[a, b]$, *if and only if* $\forall x_1 < x_2 < x_3$ in $[a, b]$

$$\begin{vmatrix} x_1 & f(x_1) & 1 \\ x_2 & f(x_2) & 1 \\ x_3 & f(x_3) & 1 \end{vmatrix} \geq 0. \tag{19}$$

We know that $x_1 \leq x_2 \leq x_3$ and $x_1, \alpha > 0$. We divide each ith row by x_i:

$$\begin{vmatrix} 1 & \frac{1}{x_1}f(x_1) & \frac{1}{x_1} \\ 1 & \frac{1}{x_2}f(x_2) & \frac{1}{x_2} \\ 1 & \frac{1}{x_3}f(x_3) & \frac{1}{x_3} \end{vmatrix} \geq 0. \tag{20}$$

After the division, we denote new variables $y_1 = \frac{1}{x_3}$, $y_2 = \frac{1}{x_2}$, and $y_3 = \frac{1}{x_2}$. One can see that $y_1 < y_2 < y_3$, because $x_1 < x_2 < x_3$. We then get

$$\begin{vmatrix} 1 & y_3 f(\frac{1}{y_3}) & y_3 \\ 1 & y_2 f(\frac{1}{y_2}) & y_2 \\ 1 & y_1 f(\frac{1}{y_1}) & y_1 \end{vmatrix} \geq 0. \tag{21}$$

Changing the first and the third row of the determinant will change the sign. Changing the third and the first columns will also change the sign. Therefore

$$\begin{vmatrix} y_1 & y_1 f(\frac{1}{y_1}) & 1 \\ y_2 & y_2 f(\frac{1}{y_2}) & 1 \\ y_3 & y_3 f(\frac{1}{y_3}) & 1 \end{vmatrix} \geq 0, \tag{22}$$

and thus we get that

$$\forall x \in [a, b],\ xf\left(\frac{1}{x}\right) \text{ is convex } \iff f(x) \text{ is convex.} \tag{23}$$

Consider the following reparameterization $\tilde{y} = \frac{y}{\alpha}$, which preserves convexity. Then

$$\begin{vmatrix} \alpha\tilde{y}_1 & \alpha\tilde{y}_1 f(\frac{\alpha}{\tilde{y}_1}) & 1 \\ \alpha\tilde{y}_2 & \alpha\tilde{y}_2 f(\frac{\alpha}{\tilde{y}_2}) & 1 \\ \alpha\tilde{y}_3 & \alpha\tilde{y}_3 f(\frac{\alpha}{\tilde{y}_3}) & 1 \end{vmatrix} \geq 0. \tag{24}$$

Division of the first and the second column by α does not change the sign of the determinant, therefore,

$$xf\left(\frac{\alpha}{x}\right) \text{ is convex } \iff f(x) \text{ is convex}, \tag{25}$$

which concludes the proof. □

A.2 Proof of Proposition 1

Proposition 1. *Consider $C = \max D_f(p||q_M)$, where $D_f(p||q_M)$ is an arbitrary f-divergence between some distribution $p(z)$ and a mixture of kernels $q_M(z) = \frac{1}{M}\sum_{j=1}^{M} K_j(z)$, and $D_f(p||q_M) < \infty$. Then, maximization of the marginal gain for the set function*

$$F(Z) = -\int f\left(\frac{p(z)}{\frac{1}{M}\sum_{j=1}^{M} K_j(z)}\right)\frac{1}{M}\sum_{m=1}^{M} K_m(z)dz + C, \tag{26}$$

at step k of a greedy algorithm corresponds to

$$\arg\max_{z_k} \Delta(z_k|Z) = \arg\min_{z_k} \mathbb{E}_{z\sim K_k(z)} f\left(\frac{p(z)}{\frac{1}{M}\sum_{j=1}^{k} K_j(z)}\right). \tag{27}$$

Proof. We aim to derive a marginal gain of adding an element defined by z_k to $\frac{1}{M}\sum_{j=1}^{k-1} K_j(z)$[1]. Let us denote $G(z) = f\left(\frac{Mp(z)}{\sum_{j=1}^{k-1} K_j(z)}\right) - f\left(\frac{Mp(z)}{\sum_{j=1}^{k} K_j(z)}\right)$. Then

$$-\int f\left(\frac{Mp(z)}{\sum_{j=1}^{k} K_j(z)}\right)\frac{1}{M}\sum_{m=1}^{k} K_m(z)dz + C + \int f\left(\frac{Mp(z)}{\sum_{j=1}^{k-1} K_j(z)}\right)\frac{1}{M}\sum_{m=1}^{k-1} K_m(z)dz - C =$$
$$\int \frac{G(z)}{M}\sum_{m=1}^{k-1} K_m(z)dz - \int f\left(\frac{Mp(z)}{\sum_{j=1}^{k} K_j(z)}\right)\frac{K_k(z)}{M}dz. \tag{28}$$

One can observe that the first term of (28) is upper-bounded by a constant, which is not dependent on z_k:

$$\int \frac{G(z)}{M}\sum_{m=1}^{k-1} K_m(z)dz \leq \int f\left(\frac{kp(z)}{\sum_{j=1}^{k-1} K_j(z)}\right)\frac{1}{M}\sum_{j=1}^{k-1} K_j(z)dz \;=\; \text{const}, \tag{29}$$

therefore, to maximize the marginal gain, one needs to maximize the second term. Consequently, we write the objective corresponding to a marginal gain as

$$\Delta(z_k|Z \setminus z_k) = -\int f\left(\frac{p(z)}{\frac{1}{M}\sum_{j=1}^{k} K_j(z)}\right) K_k(z)dz, \tag{30}$$

maximization of which is equivalent to

$$\arg\min_{z_k} \mathbb{E}_{z\sim K_k(z)} f\left(\frac{p(z)}{\frac{1}{M}\sum_{j=1}^{k} K_j(z)}\right), \tag{31}$$

which concludes the proof. □

[1]Note: $\frac{1}{M}$ is a constant, which remains unchanged at all iterations of the greedy algorithm.

B Implementation details

B.1 Weighting distribution for the diversity term

We propose the following simple heuristic, defining $p^*(x)$ as a normal distribution $\mathcal{N}(\mu_{\mathcal{D}}, \alpha \cdot \Sigma_{\mathcal{D}})$ of dimensionality, corresponding to the training data. The covariance $\Sigma_{\mathcal{D}}$ for this distribution is set to be diagonal, such that the variance for every dimension j is $\Sigma_{\mathcal{D}}[j, j] = (\alpha \cdot \sigma_j)^2$, where $\alpha > 1$ is a scaling parameter, and σ_j^2 is a variance of the dimension j computed from samples of the training dataset $\mathcal{D}$. Similarly, $\mu_{\mathcal{D}}$, the vector of expected values for every dimension, is also computed from the training data. Finally, the hyperparameter $\alpha = 5$ was found to work well, and we thus report all the experimental results with it fixed. We note that a similar technique, but for *in-distribution* data generation, has been used earlier in (Melville & Mooney, 2005).

B.2 OOD detection benchmarks

MNIST The MNIST dataset benchmark included 6 datasets: Fashion MNIST Xiao et al. (2017), DTD Cimpoi et al. (2014), Omniglot Lake et al. (2015), Gaussian noise, Bernoulli noise, and uniform noise datasets (see Table B1). We re-scaled all the images to the range of $[0, 1]$. Subsequently, we applied the same mean and standard deviation as we have applied to the original images before feeding them to the network.

CIFAR and SVHN The CIFAR and SVHN OOD benchmark included 10 different datasets. Here, we also DTD, Bernoulli noise, Gaussian noise and uniform noise datasets, and added Places 365 (Zhou et al., 2017), Tiny ImageNet (Le & Yang, 2015; Deng et al., 2009), and LSUN (Yu et al., 2015) datasets to the benchmark. For CIFAR10 as in-domain data, we added CIFAR100 and SVHN (Netzer et al., 2011) to the benchmark. For CIFAR100 – CIFAR10 and SVHN. Finally, for SVHN, we added CIFAR10 and CIFAR100 as OOD datasets, making a total of 10 OOD datasets per 1 in-distribution dataset. The details about each of the datasets are shown in Table B1.

Before feeding the images to the network, we applied re-scaling similarly to the MNIST setting. We also used the same mean and standard deviation normalization procedure, as for the in-domain data.

Table B1: Description of the datasets used in all the exp. R indicates real images, S – synthetic.

Dataset	Type	# samples	Comment
Uniform	S	$25,000$	N/A
Gaussian		$25,000$	Generated once, used in all experiments
Blobs		$25,000$	N/A
Bernoulli		$25,000$	N/A
Omniglot		$13,181$	Evaluation images
CIFAR10	R	$10,000$	Test set (not used in training)
CIFAR100		$10,000$	Test set (not used in training)
SVHN		$73,257$	Test set (not used in training)
Places 365		$10,000$	First $10,000$ images from the test set (sorted alphabetically)
TinyImageNet		$10,000$	Original validation set images
DTD		$5,640$	Release 1.0.1
LSUN		$10,000$	Test set
Fashion MNIST		$10,000$	Test set

B.3 Epistemic uncertainty computation

We used the *epistemic uncertainty*, i.e. mutual information (MI) between the label y for the point $\hat{\mathbf{x}}$ and the posterior distribution over functions $p(f|\mathcal{D})$, to evaluate the uncertainty (Malinin & Gales, 2018; Depeweg et al., 2018). As a distribution over weights induces a distribution over functions, we approximate the MI as:

$$\mathcal{I}(y; f|\hat{\mathbf{x}}, \mathcal{D}) = \mathcal{H}\left[\mathbb{E}_{p(\theta|\hat{\mathbf{x}},\mathcal{D})} p(y|\theta, \hat{\mathbf{x}}, \mathcal{D})\right] - \mathbb{E}_{p(\theta|\hat{\mathbf{x}},\mathcal{D})} \mathcal{H}\left[p(y|\theta, \hat{\mathbf{x}}, \mathcal{D})\right], \tag{32}$$

where $\mathcal{H}[\cdot]$ denotes the entropy. One can see that this metric can be efficiently computed from the predictions of an ensemble.

C Experiments

C.1 Experimental details

Model selection Contrary to the commonly used practice, we did not use CIFAR10/100 and SVHN test set sets for model selection. Neither did we use any OOD data. Instead, we used validation set accuracy (10% of the training data; randomly chosen stratified split) to select the models when optimizing the marginal gain. The best snapshot was found using the validation data, was then selected for final testing. When selecting the models for evaluation on OOD data, we first evaluated ensembles on the in-distribution test set (Appendix C.2). Subsequently, we selected the highest λ_M that did not harm the test set (in-domain) performance (no overlap of confidence intervals defined as mean $\pm$ standard error). To provide additional information, we also analyzed adaptive calibration error (ACE) with 30 bins (Nixon et al., 2019).

Two moons dataset For the synthetic data experiments, we used scikit-learn (Pedregosa et al., 2011), and generated a two-moons dataset with 300 points in total, having the noise parameter fixed to 0.3. Here, we used a two-layer neural network with ReLU (Krizhevsky, 2009) activations and hidden layer size of 128.

CIFAR10/100 and SVHN The main training hyper-parameters were adapted from (Maddox et al., 2019) (see Table C2), but with additional modifications inspired by (Malinin & Gales, 2018; Smith & Topin, 2019), which helped to train the CIFAR models to state-of-the-art performance in only 100 epochs. As such, we first employed a warm-up of the learning rate (LR) from a value 10 times lower than the initial LR (LR_{init} in Table C2) for 5 epochs. Subsequently, after 50% of the training budget, we linearly annealed the LR to the value of $LR \times lr_{scale}$ until 90% of the training budget is reached, after which we kept the value of LR constant.

All models were trained using stochastic gradient descent with momentum of 0.9 and a total batch size of 128. We employed standard training augmentations – horizontal flipping, reflective padding to 34×34, and random crop to 34×34 pixels.

Model	$\mathbf{LR_{init}}$	**Nesterov**	**Weight Decay**	lr_{scale}
PreResNet164	0.1	Yes	0.0001	0.01
VGG16BN	0.05	No	0.0005	0.01
WideResNet28x10	0.1	No	0.0005	0.001

Table C2: Main hyper-parameters of all the models used in the CIFAR and SVHN in-domain experiments.

MNIST In addition to the CIFAR10/100 experiments, we also trained our method on MNIST (LeCun et al., 1998) with PreResNet8 architecture. As OOD, we used FashionMNIST (Xiao et al., 2017) and Omniglot (Lake et al., 2015) datasets. We also tested other architectures, such as PreResNet20, but the models with higher depth than 8 already gave nearly perfect scores on MNIST.

Hyper-parameter-wise, we trained all the models for 20 epochs without warmup with the batch size of 256 using plain SGD with momentum. The weight decay was set to $1e-5$. We used LR annealing similarly as for CIFAR experiments, but used $lr_{scale} = 0.0001$. No data augmentations were used in any of the MNIST experiments. λ_M was searched in range $\{0.0001, 0.001, 0.01, 0.11, 7\}$ for $M \in \{3, 5, 9, 15\}$. This series of experiments was re-run 3 times, as the MNIST dataset is rather simple, and the test scores have low variance between the runs.

C.2 CIFAR10/100 and SVHN in-domain performance

CIFAR10/100 in-distribution performance vs. diversity. Figure C1 provides an illustration of how the test set performance changes with λ_M on CIFAR data. One can see a general trend that when λ_M approaches M, the models lose the ability to make accurate predictions, which results in lower accuracy and poorer calibration. Interestingly, performance on the VGG model degrades much slower with λ_M compared to other architectures. Similar findings were

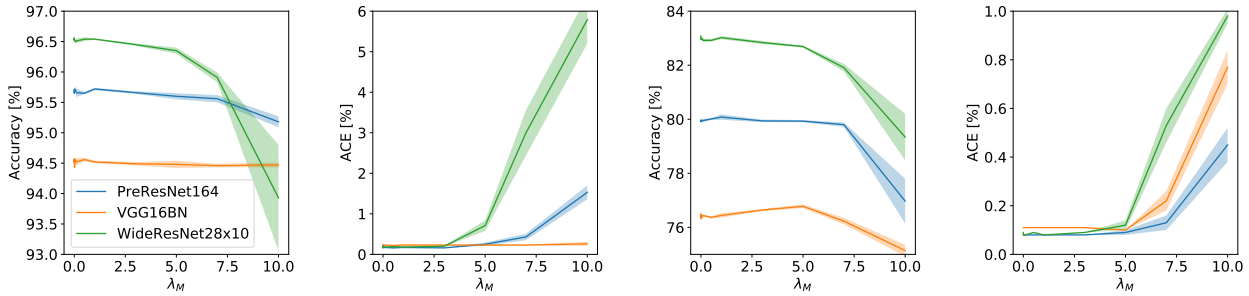

(a) (b) (c) (d)

Figure C1: Relationship between accuracy, ACE, and λ_M ($M = 11$). Subplots (a) and (b) show the results for CIFAR10. Subplots (c) and (d) show the results for CIFAR100.

also obtained for the SVHN dataset. Based on the test performance, we selected the models for further evaluation on OOD benchmark.

CIFAR and SVHN: best models' performance Table C3 shows the results of all the trained models on the in-domain data. One can see that the results between Deep Ensembles (DE) (Lakshminarayanan et al., 2017) do not differ significantly. We trained all these models according to the earlier specified hyper-parameters and the learning rate schedule. Models selected in Table C3 are used to report the results in the main experiments.

Table C3: In-domain performance on the test sets of CIFAR10/100 and SVHN for all the models used in the experiments ($M = 11$). We report mean and standard error over 5 random seeds for each of the models. Standard errors are reported if they are more than 0.01 across runs. DE indicates Deep Ensembles.

Architecture	**Dataset**	**Method**	**Accuracy (%)**	**NLL** $\times 100$	**ACE (%)**
PreResNet164	C10	DE	$95.70_{\pm 0.02}$	$13.28_{\pm 0.06}$	0.18
		Ours ($\lambda_M = 3$)	$95.66_{\pm 0.02}$	$13.18_{\pm 0.09}$	0.16
	C100	DE	$79.97_{\pm 0.04}$	$73.44_{\pm 0.17}$	0.08
		Ours ($\lambda_M = 5$)	$79.93_{\pm 0.04}$	$74.16_{\pm 0.91}$	$0.09_{\pm 0.01}$
	SVHN	DE	$99.46_{\pm 0.01}$	$2.34_{\pm 0.04}$	0.25
		Ours ($\lambda_M = 1$)	$99.38_{\pm 0.01}$	$3.16_{\pm 0.13}$	$0.81_{\pm 0.12}$
VGG16BN	C10	DE	$94.55_{\pm 0.02}$	$17.59_{\pm 0.05}$	0.23
		Ours ($\lambda_M = 5$)	$94.48_{\pm 0.06}$	$17.84_{\pm 0.15}$	$0.23_{\pm 0.01}$
	C100	DE	$76.32_{\pm 0.09}$	$91.07_{\pm 0.35}$	0.11
		Ours ($\lambda_M = 5$)	$76.78_{\pm 0.07}$	$89.10_{\pm 0.33}$	0.10
	SVHN	DE	$99.40_{\pm 0.01}$	$2.71_{\pm 0.02}$	$0.18_{\pm 0.01}$
		Ours ($\lambda_M = 1$)	$99.25_{\pm 0.01}$	$3.94_{\pm 0.10}$	$0.95_{\pm 0.12}$
WideResNet28x10	C10	DE	$96.56_{\pm 0.02}$	$10.76_{\pm 0.06}$	$0.16_{\pm 0.01}$
		Ours ($\lambda_M = 1$)	$96.54_{\pm 0.01}$	$10.99_{\pm 0.03}$	$0.18_{\pm 0.01}$
	C100	DE	$83.08_{\pm 0.09}$	$62.05_{\pm 0.18}$	0.09
		Ours ($\lambda_M = 1$)	$83.02_{\pm 0.06}$	$62.20_{\pm 0.13}$	0.08
	SVHN	DE	$99.45_{\pm 0.01}$	$2.53_{\pm 0.03}$	$0.43_{\pm 0.01}$
		Ours ($\lambda_M = 1$)	99.38	$2.87_{\pm 0.04}$	$0.46_{\pm 0.01}$

C.3 Detailed CIFAR, SVHN results

Detalized versions of the results presented in the main text are shown in Table C4. The corresponding λ_M coefficients are the same as in Table C3.

Table C4: CIFAR10 results. We report mean and standard error over 5 random seeds for each of the models. Standard errors are reported if they are more than 0.01 across runs. DE indicates Deep Ensembles.

Architecture	**OOD dataset**	**DE**			**Ours**		
		AUC (↑)	**AP (↑)**	**FPR95 (↓)**	**AUC (↑)**	**AP (↑)**	**FPR95 (↓)**
PreResNet164	bernoulli	$0.98_{\pm 0.01}$	$0.97_{\pm 0.01}$	$0.04_{\pm 0.01}$	**1.00**	**1.00**	**0.00**
	blobs	0.96	0.98	$0.12_{\pm 0.01}$	0.96	0.98	$0.12_{\pm 0.01}$
	cifar100	0.90	0.87	0.30	0.90	**0.88**	0.30
	dtd	0.93	0.83	$0.19_{\pm 0.01}$	**0.96**	**0.93**	**0.14**
	gaussian	$0.93_{\pm 0.01}$	$0.94_{\pm 0.01}$	$0.16_{\pm 0.01}$	$0.96_{\pm 0.02}$	$0.97_{\pm 0.02}$	$\mathbf{0.11_{\pm 0.03}}$
	lsun	0.93	0.89	0.20	**0.95**	**0.94**	**0.18**
	places	0.92	0.89	0.21	**0.94**	**0.93**	**0.19**
	svhn	0.94	0.99	0.16	**0.95**	0.99	**0.14**
	tiny imagenet	0.91	0.88	0.28	**0.92**	**0.89**	**0.26**
	uniform	$0.98_{\pm 0.01}$	$0.97_{\pm 0.01}$	$0.04_{\pm 0.01}$	**1.00**	**1.00**	**0.00**
VGG16BN	bernoulli	$0.94_{\pm 0.01}$	$0.95_{\pm 0.01}$	$0.11_{\pm 0.02}$	**1.00**	**1.00**	**0.00**
	blobs	0.96	0.98	0.16	0.96	0.98	**0.15**
	cifar100	0.89	0.86	0.34	0.89	0.86	0.34
	dtd	0.90	$0.77_{\pm 0.01}$	$0.25_{\pm 0.01}$	**0.96**	**0.92**	**0.18**
	gaussian	0.95	0.97	$0.14_{\pm 0.01}$	**0.99**	**0.99**	$\mathbf{0.05_{\pm 0.01}}$
	lsun	0.93	0.91	0.24	**0.95**	**0.94**	**0.21**
	places	0.91	0.90	$0.27_{\pm 0.01}$	**0.94**	**0.93**	**0.23**
	svhn	0.87	0.97	$0.28_{\pm 0.01}$	0.87	0.97	$0.27_{\pm 0.01}$
	tiny imagenet	0.90	0.88	0.33	0.90	0.88	**0.32**
	uniform	$0.90_{\pm 0.02}$	$0.89_{\pm 0.01}$	$0.16_{\pm 0.02}$	**1.00**	**1.00**	**0.00**
WideResNet28x10	bernoulli	1.00	1.00	0.00	1.00	1.00	0.00
	blobs	0.96	0.97	$0.11_{\pm 0.01}$	**0.97**	**0.98**	$0.10_{\pm 0.01}$
	cifar100	**0.92**	0.89	0.27	0.91	0.89	0.27
	dtd	0.93	$0.86_{\pm 0.01}$	$0.22_{\pm 0.01}$	**0.97**	**0.94**	$\mathbf{0.14_{\pm 0.01}}$
	gaussian	$0.96_{\pm 0.01}$	$0.97_{\pm 0.01}$	$0.09_{\pm 0.01}$	**1.00**	**1.00**	**0.00**
	lsun	0.93	0.91	0.20	**0.95**	**0.95**	$\mathbf{0.17_{\pm 0.01}}$
	places	0.93	0.91	0.21	**0.95**	**0.94**	**0.18**
	svhn	**0.96**	0.99	**0.12**	0.95	0.99	$0.13_{\pm 0.01}$
	tiny imagenet	0.92	0.90	0.27	**0.93**	**0.91**	**0.25**
	uniform	1.00	1.00	0.00	1.00	1.00	0.00

C.3.1 MNIST detailed results

In-domain performance Model selection scheme on MNIST was exactly the same as for the CIFAR10/100. We illustrate the relationship between λ_M, accuracy, and the Adaptive Calibration error (ACE) in Figure C2. One can see that λ_M remains the same even when M is increasing. Table C7 shows the detailed in-domain performance for the best λ_M, equal to 0.1.

Out of distribution detection The final OOD benchmark results on MNIST are summarized in Table C8. One can see that on MNIST, our method yields a performance boost for any size of an ensemble, even for the very small ones ($M = 3$).

C.4 Additional results

Computational overhead As noted in the main section, our method has computation overhead compared to DE, which is also a parallel method, allowing to get the results computed in $\mathcal{O}(1)$ time (in the number of models). Table C9

Table C5: CIFAR100 results. We report mean and standard error over 5 random seeds for each of the models. Standard errors are reported if they are more than 0.01 across runs. DE indicates Deep Ensembles.

Architecture	**OOD dataset**	**DE**			**Ours**		
		AUC (↑)	**AP (↑)**	**FPR95 (↓)**	**AUC (↑)**	**AP (↑)**	**FPR95 (↓)**
PreResNet164	bernoulli	$0.81_{\pm 0.03}$	$0.82_{\pm 0.03}$	$0.24_{\pm 0.04}$	**1.00**	**1.00**	**0.00**
	blobs	$0.92_{\pm 0.01}$	0.95	$0.25_{\pm 0.02}$	$0.92_{\pm 0.02}$	$0.95_{\pm 0.01}$	$0.23_{\pm 0.03}$
	cifar10	**0.80**	**0.76**	**0.57**	$0.78_{\pm 0.01}$	0.75	$0.67_{\pm 0.02}$
	dtd	$0.76_{\pm 0.01}$	$0.61_{\pm 0.01}$	$\mathbf{0.64_{\pm 0.01}}$	$\mathbf{0.80_{\pm 0.01}}$	$\mathbf{0.75_{\pm 0.01}}$	$0.78_{\pm 0.05}$
	gaussian	$0.80_{\pm 0.01}$	$0.83_{\pm 0.01}$	$0.37_{\pm 0.02}$	$\mathbf{0.95_{\pm 0.02}}$	$\mathbf{0.97_{\pm 0.01}}$	$\mathbf{0.16_{\pm 0.05}}$
	lsun	0.86	0.81	**0.45**	**0.87**	**0.85**	$0.47_{\pm 0.01}$
	places	0.82	0.77	**0.52**	**0.83**	**0.81**	$0.60_{\pm 0.03}$
	svhn	$0.80_{\pm 0.01}$	0.96	$0.55_{\pm 0.01}$	$\mathbf{0.83_{\pm 0.01}}$	0.96	$\mathbf{0.50_{\pm 0.01}}$
	tiny imagenet	0.82	0.79	**0.53**	0.82	0.79	$0.58_{\pm 0.01}$
	uniform	$0.51_{\pm 0.09}$	$0.66_{\pm 0.05}$	$0.55_{\pm 0.09}$	**1.00**	**1.00**	**0.00**
VGG16BN	bernoulli	$0.87_{\pm 0.02}$	$0.88_{\pm 0.02}$	$0.24_{\pm 0.03}$	**1.00**	**1.00**	**0.00**
	blobs	0.95	0.97	$0.16_{\pm 0.01}$	**0.97**	**0.98**	$\mathbf{0.12_{\pm 0.02}}$
	cifar10	0.78	0.73	0.63	0.78	**0.74**	$0.64_{\pm 0.01}$
	dtd	0.73	0.53	$0.62_{\pm 0.01}$	**0.86**	$\mathbf{0.80_{\pm 0.01}}$	$\mathbf{0.50_{\pm 0.01}}$
	gaussian	$0.87_{\pm 0.02}$	$0.90_{\pm 0.01}$	$0.35_{\pm 0.04}$	$\mathbf{0.95_{\pm 0.01}}$	$\mathbf{0.97_{\pm 0.01}}$	$\mathbf{0.15_{\pm 0.03}}$
	lsun	0.85	0.82	0.47	**0.90**	**0.89**	**0.40**
	places	0.82	0.78	0.55	**0.86**	**0.85**	**0.51**
	svhn	$0.76_{\pm 0.01}$	0.95	$0.67_{\pm 0.02}$	$0.76_{\pm 0.01}$	0.95	$0.72_{\pm 0.04}$
	tiny imagenet	0.81	0.78	0.56	**0.83**	**0.79**	**0.55**
	uniform	$0.86_{\pm 0.02}$	$0.89_{\pm 0.02}$	$0.28_{\pm 0.04}$	**1.00**	**1.00**	**0.00**
WideResNet28x10	bernoulli	$0.97_{\pm 0.02}$	$0.96_{\pm 0.02}$	$0.04_{\pm 0.02}$	**1.00**	**1.00**	**0.00**
	blobs	0.95	0.97	$0.16_{\pm 0.01}$	$\mathbf{0.98_{\pm 0.01}}$	**0.99**	$\mathbf{0.09_{\pm 0.02}}$
	cifar10	0.80	0.74	0.53	**0.81**	**0.76**	$0.54_{\pm 0.01}$
	dtd	$0.84_{\pm 0.01}$	$0.75_{\pm 0.01}$	$0.54_{\pm 0.01}$	$\mathbf{0.88_{\pm 0.01}}$	$\mathbf{0.84_{\pm 0.01}}$	$\mathbf{0.49_{\pm 0.02}}$
	gaussian	$0.72_{\pm 0.08}$	$0.78_{\pm 0.05}$	$0.39_{\pm 0.09}$	$\mathbf{0.94_{\pm 0.03}}$	$\mathbf{0.97_{\pm 0.01}}$	$\mathbf{0.20_{\pm 0.07}}$
	lsun	0.87	$0.81_{\pm 0.01}$	0.35	**0.91**	$\mathbf{0.90_{\pm 0.01}}$	$\mathbf{0.32_{\pm 0.01}}$
	places	0.84	$0.79_{\pm 0.01}$	$0.44_{\pm 0.01}$	**0.88**	$\mathbf{0.87_{\pm 0.01}}$	$\mathbf{0.41_{\pm 0.01}}$
	svhn	0.80	0.95	$0.52_{\pm 0.01}$	$0.80_{\pm 0.01}$	0.95	$0.52_{\pm 0.01}$
	tiny imagenet	0.84	0.78	0.46	**0.85**	**0.81**	0.46
	uniform	$0.95_{\pm 0.01}$	$0.96_{\pm 0.01}$	$0.12_{\pm 0.03}$	**1.00**	**1.00**	**0.00**

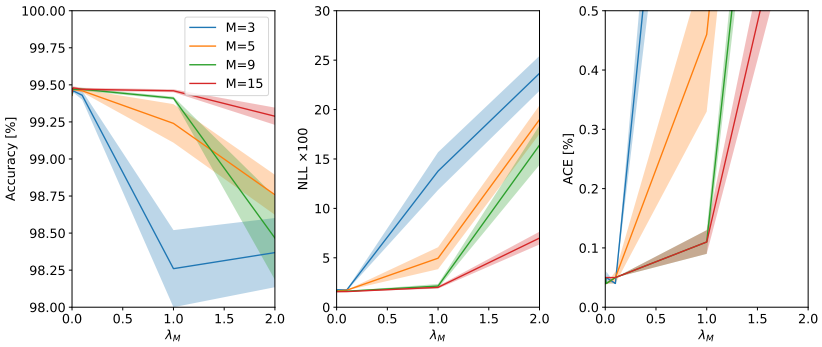

(a) (b) (c)

Figure C2: Relationship between accuracy, negative log-likelihood, ACE, and λ_M for different M on MNIST (LeCun et al., 1998). Subplots (a) and (b) show the results for PreResNet8. Experiments were rerun 3 times with different seeds. We found that the best results were obtained with $\lambda_M = 0.1$.

shows the exact walltime (WT) comparisons and the estimated computational overhead computed as

$$Overhead = \left(\frac{WT_{Ours}}{WT_{DE}} - 1 \right) \times 100\%. \tag{33}$$

Table C6: SVHN results (averaged across 5 seeds)

Architecture	OOD dataset	DE			Ours		
		AUC (↑)	AP (↑)	FPR95 (↓)	AUC (↑)	AP (↑)	FPR95 (↓)
PreResNet164	bernoulli	1.00	0.99	0.01	1.00	**1.00**	**0.00**
	blobs	**1.00**	**0.99**	**0.01**	0.99	0.98	0.02
	cifar10	0.99	0.97	0.02	0.99	0.97	0.02
	cifar100	0.99	0.96	**0.02**	0.99	0.96	0.04
	dtd	0.99	0.94	0.02	**1.00**	**0.98**	**0.01**
	gaussian	1.00	0.99	0.01	1.00	**1.00**	**0.00**
	lsun	0.99	0.96	0.02	**1.00**	**0.98**	**0.01**
	places	0.99	0.96	0.02	**1.00**	**0.98**	**0.01**
	tiny imagenet	0.99	0.96	0.02	**1.00**	**0.97**	0.02
	uniform	1.00	0.99	0.01	1.00	**1.00**	**0.00**
VGG16BN	bernoulli	1.00	0.99	0.01	1.00	**1.00**	**0.00**
	blobs	1.00	0.98	0.01	1.00	**0.99**	0.01
	cifar10	0.99	0.95	**0.02**	0.99	**0.96**	0.03
	cifar100	0.99	0.94	**0.02**	0.99	**0.95**	0.05
	dtd	0.99	0.93	0.02	**1.00**	**0.97**	**0.01**
	gaussian	1.00	0.99	0.01	1.00	**1.00**	**0.00**
	lsun	0.99	0.95	0.02	**1.00**	**0.99**	**0.01**
	places	0.99	0.96	0.02	**1.00**	**0.98**	**0.01**
	tiny imagenet	0.99	0.95	**0.02**	0.99	**0.97**	0.03
	uniform	1.00	0.99	0.01	1.00	**1.00**	**0.00**
WideResNet28x10	bernoulli	1.00	$0.99_{\pm 0.01}$	$0.02_{\pm 0.01}$	1.00	1.00	**0.00**
	blobs	0.99	0.98	0.02	**1.00**	**0.99**	**0.01**
	cifar10	0.99	0.96	0.02	**1.00**	**0.97**	0.02
	cifar100	0.99	0.95	0.03	0.99	**0.97**	**0.02**
	dtd	0.99	$0.91_{\pm 0.01}$	0.04	**1.00**	**0.99**	**0.00**
	gaussian	1.00	0.98	0.02	1.00	**1.00**	**0.00**
	lsun	0.99	0.95	0.03	**1.00**	**0.99**	**0.00**
	places	0.99	0.95	0.03	**1.00**	**0.99**	**0.00**
	tiny imagenet	0.99	0.96	0.02	**1.00**	**0.98**	**0.01**
	uniform	0.99	$0.98_{\pm 0.01}$	$0.03_{\pm 0.01}$	**1.00**	**1.00**	**0.00**

Does the choice weighting distribution for the diversity term affect the results? We considered PreResNet164 trained on CIFAR100 with CIFAR10 as a weighting distribution dataset. This approach can be seen as a form of outlier exposure technique, earlier proposed by Hendrycks et al. (2018). The results on OOD benchmark (excluding CIFAR10) are shown in Table C10. One can observe that the relationship between changing to a dataset of real images and the OOD detection performance is non-trivial. While for some datasets outlier exposure did bring benefit, for some other datasets, it did not. Notably, the datasets on which the benefit of outlier exposure was the best were datasets of real images, and we think that in case unlabeled images with non-overlapping class distribution are available, using them can bring benefit.

Effect of model capacity While the main experiments in the paper were conducted using large models, we also investigated whether ensembles of smaller models can benefit from our method. We followed the same λ_M selection procedure as for the main experiments in the paper, and report results for PreResNet20 in Table C11 for an ensemble of size $M = 11$. We found that the optimal λ_M in this case is smaller compared to λ_M for PreResNet164, and our method here does not yield any substantial boost over Deep Ensembles on these data. We found that all the models with small capacity trained on CIFAR diverged with high λ_M

Size	Method	Accuracy (%)	NLL $\times 100$	ECE (%)
3	DE	$99.44_{\pm 0.02}$	$1.72_{\pm 0.03}$	$0.23_{\pm 0.01}$
	Ours	$99.43_{\pm 0.03}$	$1.74_{\pm 0.07}$	$0.24_{\pm 0.04}$
5	DE	$99.43_{\pm 0.01}$	$1.65_{\pm 0.04}$	$0.22_{\pm 0.01}$
	Ours	$99.46_{\pm 0.01}$	$1.72_{\pm 0.02}$	$0.32_{\pm 0.01}$
7	DE	$99.44_{\pm 0.01}$	$1.61_{\pm 0.03}$	$0.25_{\pm 0.01}$
	Ours	$99.41_{\pm 0.01}$	$1.66_{\pm 0.06}$	0.28
9	DE	$99.44_{\pm 0.01}$	$1.65_{\pm 0.04}$	$0.28_{\pm 0.01}$
	Ours	$99.47_{\pm 0.01}$	$1.62_{\pm 0.03}$	$0.31_{\pm 0.01}$
15	DE	$99.47_{\pm 0.01}$	$1.60_{\pm 0.03}$	$0.29_{\pm 0.01}$
	Ours	99.49	$1.57_{\pm 0.03}$	$0.30_{\pm 0.02}$

Table C7: Test set results (in-domain performance) of our method on PreResNet8 trained on MNIST with different ensemble sizes M. We report the means over 3 random seeds for each of the models. $\lambda_M = 0.1$ Was used for all the experiments when training our method. Standard errors are reported if they are more than 0.01 across runs. DE indicates Deep Ensembles.

Robustness to distribution shift As an additional evaluation, we investigated whether our method performs on par with DE under the distribution shift, to make sure that introduction of additional regularization did not affect the robustness properties. We thus use a corrupted version of CIFAR10 test set released by (Hendrycks & Dietterich, 2019), and it has been recently shown that DE outperform many other methods on this benchmark (Ovadia et al., 2019). Here, we report the results for VGG16BN and PreResNet164, as they yielded OOD performance gain in both SVHN and LSUN datasets. One can see from Figure C3 that our method performs on-par with DE, as no statistical significance in difference between methods can be concluded from this plot. This further supports our claims that the developed greedy ensemble training approach works the same or on par with DE.

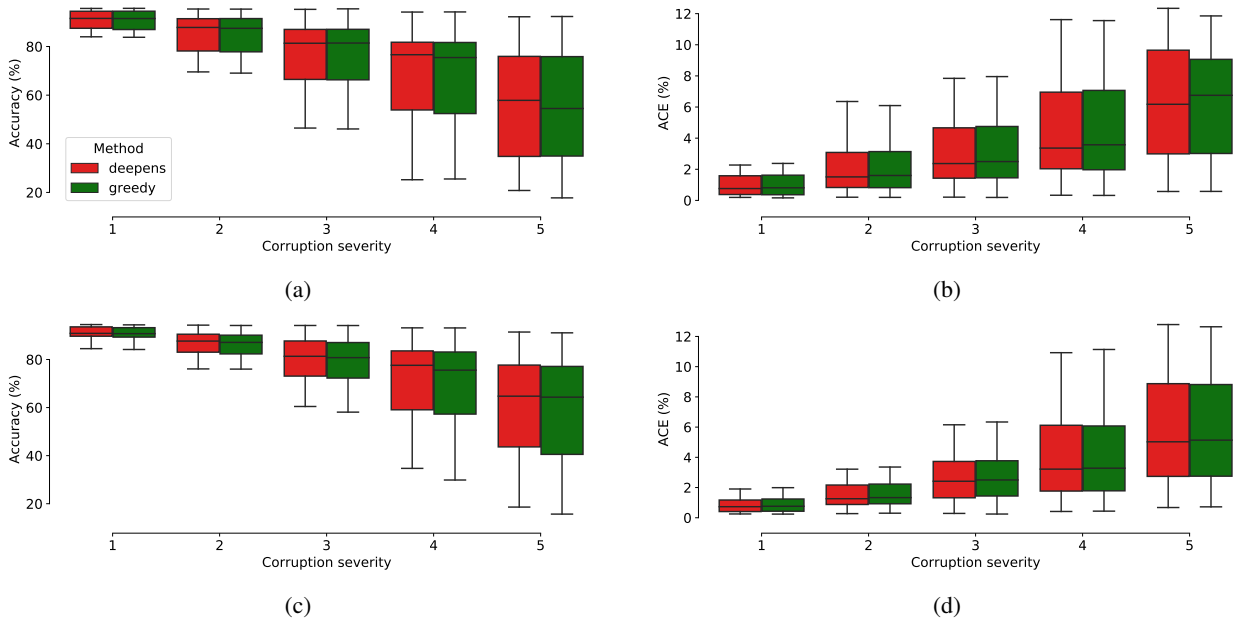

Figure C3: CIFAR10 Robustness benchmark results ($M = 11$) (Hendrycks & Dietterich, 2019). Subplots (a) and (b) show the results for PreResNet164 trained with $\lambda_M = 3$. Subplots (c) and (d) show the results for VGG16BN trained with $\lambda_M = 5$. The results have been averaged over 5 seeds.

Effect of ensemble size on CIFAR We ran our experiments using PreResNet164 with on CIFAR10/100, having $M \in \{3, 5, 7\}$ and $\lambda_M\{0.1, 0.5, 0.8, 1, 1.5, 2, 3\}$. Both in-domain accuracy, and the OOD detection on LSUN and SVHN are shown in Table C12. The results in that table show that with small ensemble size, our method may yield better performance than DE on SVHN, abut even with an ensemble of size $M = 3$, it has a substantial boost over DE in detecting LSUN.

Table C8: Out-of-distribution detection results of our method with PreResNet8 trained on MNIST with different ensemble sizes M. We report the means over 3 random seeds for each of the models. $\lambda_M = 0.1$ Was used for all the experiments when training our method. Standard errors are reported if they are more than 0.01 across runs. DE indicates Deep Ensembles.

Size	**OOD dataset**	**DE**			**Ours**		
		AUC (↑)	**AP (↑)**	**FPR95 (↓)**	**AUC (↑)**	**AP (↑)**	**FPR95 (↓)**
3	bernoulli	$0.09_{\pm 0.05}$	$0.52_{\pm 0.01}$	0.98	**1.00**	**1.00**	**0.00**
	dtd	$0.41_{\pm 0.16}$	$0.47_{\pm 0.13}$	$0.97_{\pm 0.01}$	**1.00**	**0.99**	**0.00**
	fashion mnist	$0.89_{\pm 0.03}$	$0.92_{\pm 0.02}$	$0.71_{\pm 0.19}$	$\mathbf{0.99_{\pm 0.01}}$	**0.99**	$\mathbf{0.07_{\pm 0.03}}$
	gaussian	$0.98_{\pm 0.01}$	$0.99_{\pm 0.01}$	$0.06_{\pm 0.02}$	$0.99_{\pm 0.01}$	1.00	$0.03_{\pm 0.02}$
	omniglot	0.98	0.98	0.08	0.98	0.98	0.08
	uniform	$0.23_{\pm 0.17}$	$0.58_{\pm 0.07}$	$0.90_{\pm 0.06}$	**1.00**	**1.00**	**0.00**
5	bernoulli	0.02	0.50	0.98	**1.00**	**1.00**	**0.00**
	dtd	$0.48_{\pm 0.17}$	$0.55_{\pm 0.14}$	$0.94_{\pm 0.03}$	**1.00**	**1.00**	**0.00**
	fashion mnist	$0.87_{\pm 0.05}$	$0.92_{\pm 0.03}$	$0.67_{\pm 0.24}$	**0.99**	**0.99**	$\mathbf{0.04_{\pm 0.01}}$
	gaussian	1.00	1.00	$0.02_{\pm 0.01}$	1.00	1.00	$0.01_{\pm 0.01}$
	omniglot	0.98	0.99	**0.06**	0.98	0.99	0.07
	uniform	$0.30_{\pm 0.22}$	$0.62_{\pm 0.10}$	$0.77_{\pm 0.18}$	**1.00**	**1.00**	**0.00**
7	bernoulli	$0.33_{\pm 0.24}$	$0.66_{\pm 0.13}$	$0.77_{\pm 0.18}$	**1.00**	**1.00**	**0.00**
	dtd	$0.75_{\pm 0.12}$	$0.76_{\pm 0.11}$	$0.67_{\pm 0.25}$	**1.00**	**1.00**	**0.00**
	fashion mnist	$0.95_{\pm 0.02}$	$0.97_{\pm 0.02}$	$0.29_{\pm 0.18}$	**0.99**	0.99	$\mathbf{0.05_{\pm 0.01}}$
	gaussian	1.00	1.00	$0.02_{\pm 0.01}$	1.00	1.00	$0.02_{\pm 0.01}$
	omniglot	0.99	0.99	0.06	0.99	0.99	$0.06_{\pm 0.01}$
	uniform	$0.49_{\pm 0.22}$	$0.71_{\pm 0.12}$	$0.64_{\pm 0.26}$	**1.00**	**1.00**	**0.00**
9	bernoulli	$0.45_{\pm 0.17}$	$0.70_{\pm 0.08}$	$0.90_{\pm 0.05}$	**1.00**	**1.00**	**0.00**
	dtd	$0.83_{\pm 0.06}$	$0.83_{\pm 0.06}$	$0.68_{\pm 0.23}$	**1.00**	**1.00**	**0.00**
	fashion mnist	$0.97_{\pm 0.01}$	0.97	$0.16_{\pm 0.04}$	**1.00**	**1.00**	**0.01**
	gaussian	1.00	1.00	$0.01_{\pm 0.01}$	1.00	1.00	0.00
	omniglot	0.99	0.99	0.06	0.99	0.99	0.06
	uniform	$0.72_{\pm 0.15}$	$0.82_{\pm 0.09}$	$0.50_{\pm 0.21}$	**1.00**	**1.00**	**0.00**
15	bernoulli	$0.18_{\pm 0.06}$	$0.55_{\pm 0.02}$	$0.99_{\pm 0.01}$	**1.00**	**1.00**	**0.00**
	dtd	$0.82_{\pm 0.04}$	$0.80_{\pm 0.04}$	$0.84_{\pm 0.09}$	**1.00**	**1.00**	**0.00**
	fashion mnist	0.97	0.97	$0.17_{\pm 0.03}$	**1.00**	**1.00**	**0.01**
	gaussian	1.00	1.00	$0.01_{\pm 0.01}$	1.00	1.00	$0.01_{\pm 0.01}$
	omniglot	0.99	0.99	0.05	0.99	0.99	0.05
	uniform	$0.70_{\pm 0.13}$	$0.80_{\pm 0.07}$	$0.53_{\pm 0.19}$	**1.00**	**1.00**	**0.00**

Qualitative results on CIFAR100. In Figure C4, we further illustrate the capabilities of uncertainty estimation of our method for the PreResNet164 trained on CIFAR100 ($M = 11$). Our method has a better true positive rate (as can also be seen from the histograms), and slightly better precision when the threshold for the recall is high. We note that

Table C9: Walltime comparisons of Deep Ensembles and our method for $M = 11$ on CIFAR10 for 3 architectures. Both methods have been trained on 1 GPU for fair estimation of the computational overhead. The results reported over five runs with different random seeds.

Architecture	**Walltime (hours)**		**Overhead**
	DE	**Ours**	
PreResNet164	18.81±0.18	32.81±0.25	74.39%
VGG16BN	2.11±0.01	4.00±0.03	89.12%
WideResNet28x10	23.23±0.07	43.92±0.25	89.03%

Table C10: Outlier exposure results for PreResNet164 trained on CIFAR100 with CIFAR10 as a weighting distribution for the diversity term. We found $\lambda_M = 1$ to be the best one for this experiment in the outlier exposure. The most optimal setting for our model was $\lambda_M = 3$ and $\lambda_M = 5$, respectively.

OOD dataset	DE			Ours			Ours w. Outlier Exposure		
	AUC (↑)	AP (↑)	FPR95 (↓)	AUC (↑)	AP (↑)	FPR95 (↓)	AUC (↑)	AP (↑)	FPR95 (↓)
bernoulli	$0.81_{\pm 0.03}$	$0.82_{\pm 0.03}$	$0.24_{\pm 0.04}$	**1.00**	**1.00**	**0.00**	**1.00**	**1.00**	0.00
blobs	$0.92_{\pm 0.01}$	0.95	$0.25_{\pm 0.02}$	$0.92_{\pm 0.02}$	$0.95_{\pm 0.01}$	$0.23_{\pm 0.03}$	$\mathbf{0.96_{\pm 0.01}}$	**0.98**	$\mathbf{0.14_{\pm 0.01}}$
dtd	$0.76_{\pm 0.01}$	$0.61_{\pm 0.01}$	$0.64_{\pm 0.01}$	$\mathbf{0.80_{\pm 0.01}}$	$\mathbf{0.75_{\pm 0.01}}$	$0.78_{\pm 0.05}$	$\mathbf{0.81_{\pm 0.01}}$	$0.71_{\pm 0.01}$	**0.57**
gaussian	$0.80_{\pm 0.01}$	$0.83_{\pm 0.01}$	$0.37_{\pm 0.02}$	$\mathbf{0.95_{\pm 0.02}}$	$\mathbf{0.97_{\pm 0.01}}$	$\mathbf{0.16_{\pm 0.05}}$	$0.94_{\pm 0.01}$	$0.96_{\pm 0.01}$	$0.19_{\pm 0.03}$
lsun	0.86	0.81	0.45	0.87	0.85	$0.47_{\pm 0.01}$	**0.89**	$\mathbf{0.88_{\pm 0.01}}$	$\mathbf{0.40_{\pm 0.01}}$
places	0.82	0.77	0.52	0.83	0.81	$0.60_{\pm 0.03}$	**0.86**	$\mathbf{0.84_{\pm 0.01}}$	$\mathbf{0.49_{\pm 0.01}}$
svhn	$0.80_{\pm 0.01}$	0.96	$0.55_{\pm 0.01}$	$\mathbf{0.83_{\pm 0.01}}$	0.96	$\mathbf{0.50_{\pm 0.01}}$	$0.78_{\pm 0.01}$	0.95	$0.56_{\pm 0.02}$
tiny imagenet	0.82	0.79	**0.53**	0.82	0.79	$0.58_{\pm 0.01}$	**0.83**	0.79	**0.52**
uniform	$0.51_{\pm 0.09}$	$0.66_{\pm 0.05}$	$0.55_{\pm 0.09}$	**1.00**	**1.00**	**0.00**	$0.98_{\pm 0.01}$	$0.98_{\pm 0.02}$	$0.05_{\pm 0.02}$

Table C11: Out of distribution detection for a small-capacity model – PreResNet20 ($M = 11$). Results were averaged over 5 random seeds. Standard errors are not reported if they less than 0.01 across runs. DE indicates Deep Ensembles.

Dataset	OOD dataset	DE			Ours		
		AUC (↑)	AP (↑)	FPR95 (↓)	AUC (↑)	AP (↑)	FPR95 (↓)
C10	bernoulli	$0.99_{\pm 0.01}$	$0.99_{\pm 0.01}$	$0.05_{\pm 0.02}$	1.00	1.00	**0.00**
	blobs	0.97	0.98	0.12	0.97	0.98	$0.12_{\pm 0.01}$
	cifar100	0.88	0.86	0.37	**0.89**	0.86	**0.36**
	dtd	0.93	$0.86_{\pm 0.01}$	$0.22_{\pm 0.01}$	$0.94_{\pm 0.01}$	$\mathbf{0.89_{\pm 0.01}}$	$0.20_{\pm 0.01}$
	gaussian	$0.94_{\pm 0.01}$	$0.96_{\pm 0.01}$	$0.18_{\pm 0.03}$	$0.95_{\pm 0.01}$	$0.97_{\pm 0.01}$	$0.15_{\pm 0.03}$
	lsun	0.93	0.92	0.25	**0.94**	**0.93**	$\mathbf{0.23_{\pm 0.01}}$
	places	0.92	0.90	0.27	**0.93**	**0.91**	**0.26**
	svhn	$0.91_{\pm 0.01}$	0.98	$0.23_{\pm 0.01}$	0.91	0.98	$0.23_{\pm 0.01}$
	tiny imagenet	0.90	0.88	0.33	0.90	0.88	**0.32**
	uniform	0.99	0.99	$0.03_{\pm 0.01}$	**1.00**	**1.00**	**0.00**
C100	bernoulli	$0.91_{\pm 0.05}$	$0.93_{\pm 0.04}$	$0.19_{\pm 0.08}$	**1.00**	**1.00**	**0.00**
	blobs	0.95	0.97	$0.17_{\pm 0.01}$	**0.97**	**0.98**	**0.12**
	cifar10	**0.78**	**0.73**	0.63	0.77	0.72	0.63
	dtd	$0.81_{\pm 0.01}$	$0.72_{\pm 0.01}$	$0.66_{\pm 0.03}$	$0.83_{\pm 0.01}$	$\mathbf{0.77_{\pm 0.01}}$	$0.63_{\pm 0.03}$
	gaussian	$0.98_{\pm 0.01}$	0.99	$0.07_{\pm 0.01}$	0.99	0.99	$\mathbf{0.04_{\pm 0.01}}$
	lsun	0.88	0.87	$0.43_{\pm 0.01}$	**0.89**	**0.88**	$0.41_{\pm 0.01}$
	places	0.84	0.82	$0.55_{\pm 0.01}$	**0.85**	**0.83**	$\mathbf{0.52_{\pm 0.01}}$
	svhn	0.85	0.97	$0.48_{\pm 0.01}$	$0.84_{\pm 0.01}$	0.97	$0.49_{\pm 0.02}$
	tiny imagenet	0.82	0.78	0.56	0.82	**0.79**	**0.54**
	uniform	$0.90_{\pm 0.03}$	$0.92_{\pm 0.02}$	$0.23_{\pm 0.07}$	**1.00**	**1.00**	**0.00**

the histograms of epistemic uncertainties still overlap significantly, however, with our method, the model does not have a high number of overconfident predictions coming from the OOD data anymore.

Table C12: Test set and OOD detection performances on PreResNet164 for ensemble sizes $M \in \{3, 5, 7\}$. We report the means over 5 different seeds. Standard errors are reported if they are non-zero across the runs.

M	Dataset	Method	Accuracy (%)	NLL $\times 100$	ACE (%)	SVHN		LSUN	
						AUC (↑)	AP (↑)	AUC (↑)	AP (↑)
3	C10	DE	$95.38_{\pm 0.04}$	$15.59_{\pm 0.14}$	$0.25_{\pm 0.01}$	0.93	0.95	0.92	0.87
		Ours	$95.32_{\pm 0.04}$	$15.67_{\pm 0.11}$	$0.24_{\pm 0.01}$	$0.94_{\pm 0.01}$	$0.96_{\pm 0.01}$	**0.94**	$\mathbf{0.91_{\pm 0.01}}$
	C100	DE	$78.67_{\pm 0.04}$	$84.35_{\pm 0.19}$	0.10	$0.78_{\pm 0.02}$	$0.87_{\pm 0.01}$	0.82	$0.76_{\pm 0.01}$
		Ours	$78.51_{\pm 0.16}$	$84.55_{\pm 0.76}$	0.10	$0.76_{\pm 0.02}$	$0.86_{\pm 0.01}$	$0.82_{\pm 0.02}$	$0.76_{\pm 0.02}$
5	C10	DE	$95.55_{\pm 0.03}$	$14.14_{\pm 0.14}$	$0.20_{\pm 0.01}$	0.93	0.96	0.92	0.88
		Ours	$95.58_{\pm 0.04}$	$14.31_{\pm 0.07}$	0.19	**0.94**	0.96	**0.95**	**0.93**
	C100	DE	$79.50_{\pm 0.08}$	$78.85_{\pm 0.28}$	0.09	$0.78_{\pm 0.01}$	$0.87_{\pm 0.01}$	0.84	0.79
		Ours	79.33 ± 0.13	$78.59_{\pm 0.33}$	0.09	$0.80_{\pm 0.01}$	0.88	**0.86**	$\mathbf{0.82_{\pm 0.01}}$
7	C10	DE	$95.64_{\pm 0.04}$	$13.79_{\pm 0.06}$	0.19	0.94	0.96	0.92	0.88
		Ours	$95.62_{\pm 0.04}$	$14.07_{\pm 0.19}$	$0.22_{\pm 0.04}$	0.94	0.96	**0.94**	$\mathbf{0.93_{\pm 0.01}}$
	C100	DE	$79.81_{\pm 0.06}$	$76.12_{\pm 0.22}$	0.08	$0.78_{\pm 0.01}$	$0.87_{\pm 0.01}$	0.85	0.79
		Ours	$79.76_{\pm 0.08}$	$78.09_{\pm 1.41}$	$0.11_{\pm 0.02}$	$0.78_{\pm 0.01}$	$0.88_{\pm 0.01}$	**0.86**	$\mathbf{0.83_{\pm 0.01}}$

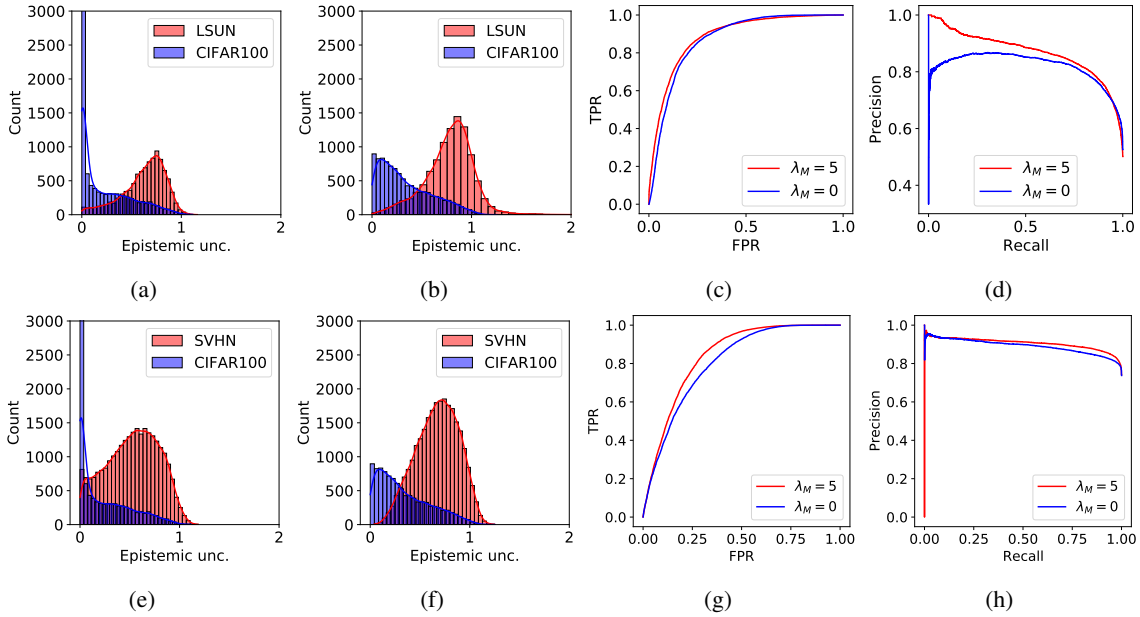

Figure C4: Uncertainty estimation quality on PreResNet164 (He et al., 2016) trained on CIFAR100 and evaluated on CIFAR100 test set vs LSUN and SVHN, respectively. Histograms (a) and (e) indicate Deep Ensembles (Lakshminarayanan et al., 2017). Histograms (b) and (f) show our method trained with $\lambda_M = 5$. Subplots (c) and (d) show the ROC and PR curves for the LSUN dataset, respectively. Subplots (g) and (h) show the ROC and PR curves for the SVHN dataset, respectively The curves were computed using average epistemic uncertainty per sample (5 seeds). Standard errors were < 0.01.